Isolation, in-vitro Cytotoxicity and in Silico Analysis of Polymethoxyflavones From Kaempferia Parviflora on Breast Cancer Cell Lines

Mohammad Aidiel
Management & Science University, Shah Alam
Maisarah Abdul Mutalib
maisarah_abdulmutalib@msu.edu.my

Management & Science University, Shah Alam

Article

Keywords: Kaempferia parviflora, isolation, Polymethoxyflavones, anticancer, multitargeted molecular docking, DFT, drug-likeness, ADMET

Posted Date: December 19th, 2025

DOI: https://doi.org/10.21203/rs.3.rs-8155038/v1

Additional Declarations: No competing interests reported.

ISOLATION, *IN-VITRO* CYTOTOXICITY AND *IN SILICO* ANALYSIS OF POLYMETHOXYFLAVONES FROM *KAEMPFERIA PARVIFLORA* ON BREAST CANCER CELL LINES

[1]Mohammad Aidiel and [1*]Maisarah Abdul Mutalib

[1]School of Graduate Studies, Management & Science University, University Drive, Off Persiaran Olahraga, Section 13, 40100, Shah Alam, Selangor, Malaysia

***Email**: maisarah_abdulmutalib@msu.edu.my

Abstract

Kaempferia parviflora (*K. parviflora*) is a plant native to Southeast Asia known for its numerous health benefits, primarily attributed to its major constituents, polymethoxyflavones (PMFs). This study aims to isolate and characterize PMFs from *K. parviflora*, evaluate their cytotoxic activity against breast cancer cell lines, and perform *in silico* analyses to explore their potential mechanisms of action. PMFs were isolated from the optimized ethanolic extract of *K. parviflora* using gravitational column chromatography, followed by structural characterization via ^{1}H-NMR and ^{13}C-NMR spectroscopy. The cytotoxic activity of the isolated PMFs was evaluated *in-vitro* against hormone-dependent MCF-7 and hormone-independent MDA-MB-231 breast cancer cell lines, as well as NIH/3T3 mouse fibroblast cells using cytotoxicity assay. *In silico* analyses included molecular docking, density functional theory (DFT) calculations, drug-likeness evaluation, ADMET screening, and Pearson correlation analysis. Nine PMFs were successfully isolated and identified: 5-hydroxy-3,7-dimethoxyflavone (**1**), 5-hydroxy-7-methoxyflavone (**2**), 5-hydroxy-3,7,4'-trimethoxyflavone (**3**), 5-hydroxy-7,4'-dimethoxyflavone (**4**), 5-hydroxy-3,7,3',4'-tetramethoxyflavone (**5**), 3,5,7-trimethoxyflavone (**6**), 5,7-dimethoxyflavone (**7**), 3,5,7,3',4'-pentamethoxyflavone (**8**), and 5,7,4'-trimethoxyflavone (**9**). All PMFs exhibited selective cytotoxicity, with stronger IC_{50} effects on MCF-7 than on MDA-MB-231 cells after 72-hour treatment. **PMF 4** showed the strongest cytotoxic effect, with an IC_{50} value of 24.12 ± 0.45 µM respectively. Toxicity screening of these PMFs on NIH-3T3 mouse fibroblast cells at their respective IC_{50} concentrations showed >80% cell viability (**PMF 9**: 88.41%) validating their selective cytotoxicity against cancer cells. **PMF 4**, **7**, and **9** demonstrated strong binding affinities across six protein targets, particularly Bcl-XL, Bcl-2, and mTOR. DFT analysis revealed stabilized PMFs with favorable frontier molecular orbitals, indicating strong electron-accepting capabilities. Drug-likeness and ADMET screening supported the bioavailability and safety profiles of the PMFs. Pearson correlation analysis showed a significant positive correlation between cytotoxic activity (IC_{50}) and binding affinity to Bcl-XL ($r = 0.831$) and mTOR ($r = 0.860$).

Keywords: *Kaempferia parviflora*, isolation, Polymethoxyflavones, anticancer, multitargeted molecular docking, DFT, drug-likeness, ADMET

Introduction

Natural products have well-documented history of providing diverse and complex chemical structures with valuable pharmacological properties, making them a rich source for drug discovery. Extensive research has transformed traditional plant-based remedies into modern, alternative, and complementary treatments, utilizing various parts of plant for diverse therapeutic applications targeting multiple biological pathways. These advancements are particularly notable in areas like diabetes (Hadi et al., 2025), cancer (Mutalib et al., 2023), inflammation (Jamtsho et al., 2024), neurological disorders (Lim

et al., 2024), and antioxidant (Shariff et al., 2020). The discovery of biologically active compounds within a living organism have served as the basis for many medicines and continue to offer new opportunities for therapeutic development. Natural products compound generally rich in carbon, oxygen and hydrogen atoms, which its combination leading to the presence of diverse functional groups such as hydroxyl, carbonyl, methoxy, alkoxy and aromatic rings (Ertl, 2021; Atanasov et al., 2021). The initial discovery of natural compounds serves as a foundation for designing new derivatives by introducing functional groups such as halogens (e.g., fluorine), as well as heteroatoms like nitrogen and sulfur, common features in alkaloids (Ding & Xue, 2024; Huo et al., 2023). This strategy enables the structural diversification of bioactive molecules, potentially enhancing their potency, pharmacokinetic, and overall drug-likeness, as demonstrated in many commercialized drugs today.

Kaempferia parviflora (K. parviflora) is a perennial herbaceous species originating from Thailand and native to Southeast Asia. Commonly known as black ginger, its rhizome has been widely used in traditional medicine for the treatment of osteoarthritis, ulcers, inflammation, gout, allergies, and other ailments (Aidiel et al., 2023; Chen et al., 2018). The extract of *K. parviflora* is rich in secondary metabolites, with flavonoids specifically polymethoxyflavones (PMFs) being the most abundant. Both the *K. parviflora* extract and its major compounds, PMFs, have demonstrated a wide range of pharmacological activities, including anticancer (Paramee et al., 2018), antioxidant (Lee et al., 2018), antimicrobial (Sitthichai et al., 2022), antibacterial (Sookkhee et al., 2022), anti-inflammatory (Phung et al., 2021), anti-acetylcholinesterase (Seo et al., 2017), and antidiabetic effects (Yagi et al., 2019). The extract exhibits potent anticancer properties through multiple pathways, including the modulation of MMP-2 and MMP-9 activity, ERK1/2, PI3K, and AKT signaling proteins, as well as IL-6 and MCP-1 gene expression, MCL-1 protein levels, and the activation of caspase-dependent apoptosis (Paramee et al., 2018; Thaklaewphan et al., 2021; Suradej et al., 2019). Although recent studies have highlighted the strong anticancer potential of *K. parviflora* extract, there is limited information regarding the specific PMF constituents responsible for its cytotoxic effects. Therefore, elucidating the anticancer mechanisms of PMFs as key bioactive secondary metabolites is essential to better understand the chemotherapeutic potential of *K. parviflora* extract.

Polymethoxyflavones (PMFs) are found in various plant species and have demonstrated significant therapeutic potential (Mushtaq et al., 2023; Peng et al., 2022). Due to the limited reports on the anticancer activity of PMFs specifically from *Kaempferia parviflora* extract, insights from PMFs derived from other natural products have helped hypothesize their potential in inducing cancer cell death, particularly in breast cancer cell lines. Recent reviews suggest that PMFs exhibit a multi-targeted mechanism of action, simultaneously activating and suppressing key protein markers involved in cancer cell apoptosis (Aidiel et al., 2025). Moreover, the synergy effects of multiple functional groups at distinct positions within the PMF structure, especially the presence of hydroxy moieties have been linked to enhanced cytotoxicity against cancer cells (Łodyga-Chruścińska et al., 2019). Computational tools have increasingly been employed to predict ligand-protein interactions and binding affinities, offering insight into the potential modulatory effects of small molecules on specific protein biomarkers (Agu et al., 2023). The emergence of structure-based inverse molecular docking and multitargeted docking approaches has greatly aided researchers in accurately identifying relevant protein targets prior to *in vitro* and *in vivo* validation (Elkhalifa et al., 2023; Acharya et al., 2019). Therefore, applying in silico techniques particularly multitargeted molecular docking offers a rapid and cost-effective strategy for preliminary screening of biomarkers involved in apoptotic pathways. This study sought to identify and isolate bioactive PMFs from the optimized *Kaempferia parviflora* ethanolic extract, evaluate their anticancer activity against breast cancer cell lines, and perform comprehensive *in silico* analyses, including molecular docking, density functional theory (DFT), and ADMET predictions. The study aims

to discover potent PMFs capable of inducing cytotoxic effects in breast cancer cells by specifically targeting key apoptotic markers involved in cancer pathogenesis.

2 Methodology

2.1 Chemicals

All chemicals, reagents and solvents were purchased from Chemiz (UK). Standard PMFs compounds were obtained from Targetmol (USA).

2.2 Plant materials

Kaempferia parviflora rhizome originating from Thailand were purchased from a supplier in Kelantan, Malaysia. The identification of the rhizome was confirmed by a botanist from the Herbarium Biodiversity Unit, Institute of Bioscience, Universiti Putra Malaysia with voucher specimen KM0071/23.

2.3 Extraction

Bulk extraction of *K. parviflora* rhizome (1000 g) was carried out at room temperature in the dark based on optimized parameters from a previous study (Aidiel et al. 2024). The filtered extract was dried under reduced pressure using a rotary evaporator, followed by freeze-drying overnight to form a dark purple amorphous powder. The final yield obtained was 109.57 g, approximately 11.05 %. The dried powder was sealed tightly to prevent moisture exposure and stored below 4 °C for future analysis. The dried *K. parviflora* extract was suspended in 150 ml ethanolic solution (50%, diluted with distilled water) and partitioned with 150 ml of n-hexane, chloroform and water successively (at least three times), until the final fraction turned colorless. Subsequently, all fractions were then concentrated under reduced pressure and weighed using an analytical balance.

2.4 Isolation and characterization

The hexane fraction (8.78 g) and chloroform fraction (24.56 g), which contained the highest PMFs content were subjected to silica gel column chromatography (70-230 mesh; Macherey-Nagel, Germany). The hexane fraction (C1) was eluted gradually in increasing polarity by n-hexane/ ethyl acetate solvent system [10:0] → [8:2] yielding eight sub-fractions (C1-1 to C1-8). Sub-fractions C1-4 (0.1927 g) and C1-5 (0.1132 g) were confirmed to yield **PMF 1** (5-hydroxy-3,7-dimethoxyflavone) (351.6 mg).

The chloroform fraction was divided to 3 major fraction (C2, C3 & C4), with all fraction eluted in multiple solvent system, from n-hexane/ethyl acetate solvent system [10:0] → [0:10], followed by ethyl acetate/dichloromethane/acetone [10:0:0] → [5:4:1] → [4:4:2] → [2:4:4] → [0:4:6] to yield 172 subfraction of **C2**, 143 subfraction of **C3** and 89 subfraction of **C4**. Subsequent re-isolation of all subfractions were performed using silica gel column chromatography (230-400 mesh; Macherey-Nagel, Germany). From major subfraction C2, the C2-5 to C2-18 subfraction were combined and reisolated with n-hexane/ethyl acetate solvent system [10:0] → [9.75:0.25] to yield **PMF 1** (53.4 mg) and **PMF 2**, 5-hydroxy-7-methoxyflavone (78.6 mg). Next, C2-19 to C2-28 subfraction were reisolated with n-hexane/ethyl acetate [10:0] → [9:1] to yield **PMF 3**; 5-hydroxy-3,7,4'-trimethoxyflavone (106.7 mg).

Combination and reisolating of C2-29 to C2-42 with n-Hexane/ethyl acetate [10:0] → [5:5] yielded **PMF 2** (2.4 mg), **PMF 3** (66.8 mg) and **PMF 4**; 5-hydroxy-7,4'-dimethoxyflavone (104.8 mg). Subfraction C2-49 to C2-52 were combined and separated by column chromatography with solvent system of n-hexane/ethyl acetate [10:0] → [5:5] to yield **PMF 5**; 5-hydroxy-3,7,3',4'-tetramethoxyflavone (32.1 mg). The subfraction from C2-167 to C2-172 were reisolated with n-hexane/acetone [10:0] → [0:10] to yield **PMF 9**; 5,7,4'-trimethoxyflavone (397.8 mg). For C3 major subfraction, the purification of subfraction C3-13 to C3-29 with n-hexane/ethyl acetate [10:0] → [9.5:0.5] successfully isolate **PMF 1** (128.2 mg), followed by **PMF 2** (46.3 mg) and **PMF 3** (69.8 mg). Subfraction C3-93 to C3-102 were isolated by two distinct solvent system, by using n-hexane/ethyl acetate [10:0] → [0:10] solvent ratio, followed by n-hexane/acetone [10:0] → [8:2] to yield **PMF 6**; 3,5,7-trimethoxyflavone (111.8 mg). Subfraction C3-119 and C3-120 were reisolated with n-hexane/acetone [10:0] → [7.5:2.5] to yield **PMF 9** (55.3 mg). Reisolating subfraction C3-136 to C3-141 by n-hexane/acetone [10:0] → [0:10] solvent ratio yielded **PMF 9** (124.4 mg). Purification of C4 major subfractions began with the reisolation of C4-10 to C4-18 subfraction with n-hexane/ethyl acetate solvent ratio of [10:0] → [9:1] yielded **PMF 1** (52.3 mg), subsequently **PMF 2** (42.2 mg) and **PMF 3** (55.4 mg). Subfraction C4-88 and C4-89 were combined and reisolated using n-hexane/acetone [10:0] → [7.5:2.5] to yield **PMF 7**; 5,7-dimethoxyflavone (104.2 mg). Lastly, subfraction C4-86 was reisolated with n-hexane/ethyl acetate solvent system [10:0] → [7.5:2.5] to yield **PMF 8**; 3,5,7,3',4'-pentamethoxyflavone (44.8 mg). The purity of isolated PMF compounds were confirmed by characterization using one-dimensional (1D) ^{1}H-NMR and ^{13}C-NMR Jeol ECZS 400 MHz instrument (Kyoto, Japan) from the Institute of Science, Universiti Teknologi Mara (UITM). Deuterated chloroform ($CDCl_3$) was used as a solvent to dissolve isolated **PMF 1** to **6**. Meanwhile, **PMF 7** to **9** was dissolved using deuterated acetone (acetone-d6). Proton and carbon chemical shifts were reported in parts per million (ppm), as visualized in supplementary materials (**Figure S1 – S18**). The purity and structure of all isolated **PMF 1** to **9** were validated from a study by Sae-wong et al. (2011). Additionally, the purity of **PMF 2**, **4**, **6**, **7**, **8**, and **9** was further reaffirmed through spectral data comparison with study by Yoshida et al. (2020). Meanwhile, spectral data of **PMF 1**, **3** and **5** was validated from a study by Luan et al. (2020), Macedo et al. (2019) and Sae-wong et al. (2009), respectively.

2.5 Cell culture

MCF-7, MDA-MB-231 and NIH-3T3 cell lines were obtained from the American Type Culture Collection (ATCC, Manassas, VA, USA), with contribution from the Immunology Unit, Faculty of Medical and Health Science, Universiti Putra Malaysia. The MCF-7 breast cancer cells and NIH-3T3 mouse fibroblast were cultured in Roswell Park Memorial Institute (RPMI) 1640 medium (Elabscience, USA) supplemented with 10% fetal bovine serum (Capricorn Scientific GmbH (Germany) and 1% penicillin/streptomycin (Elabscience, USA). Meanwhile, MDA-MB-231 breast cancer cells were cultured using Dulbecco's Modified Eagle Medium (DMEM) media. All cell lines were incubated at 37°C supplemented in a humidified atmosphere containing 5% CO_2.

2.6 3-[4,5-dimethylthiazol-2-yl]-2,5 diphenyl tetrazolium bromide (MTT) colorimetric assay

The cytotoxicity screening of PMFs isolated from *K. parviflora* extract on MCF-7 and MDA-MB-231 breast cancer cell lines and NIH-3T3 mouse fibroblast was performed using MTT colorimetric assay. MCF-7 and and MDA-MB-231 breast cancer cell lines were seeded in 96-well plates at a cell density of 5 x 10^4 cells/mL and 3 x 10^4 cells/mL, respectively. Meanwhile, NIH-3T3 mouse fibroblast were

seeded in a 96-well plate with a cell density of 1 x 10^5 cells/mL. All cells were incubated for 24 hours to reach 70-80% confluency. A stock solution of highly concentrated PMFs (40 mM) was prepared in DMSO, then diluted in a complete RPMI and DMEM medium to a non-toxic final concentration of <0.5% DMSO upon treatment. The cells were treated with various concentrations of isolated PMFs (10 – 200 µM), a positive control (doxorubicin; 0.5 – 8 µM), a vehicle control (0.5% DMSO) and a negative control (medium only). The cells were incubated for 24-, 48- and 72-hour treatment duration at 37°C, in a humidified atmosphere with 5% CO_2. After treatment, the culture medium was discarded and 100 µL of MTT solution (0.5 mg/mL in PBS) was added into the treated wells and incubated for 3 hours at 37°C. After incubation, the MTT solution was carefully removed and 100 µL DMSO was added into the well to dissolve the purple formazan crystals. The absorbance of the dissolved purple formazan crystals was measured using a microplate reader at optimized wavelength of 492 nm. The cytotoxicity of the PMFs (IC_{50}) were confirmed by determining the concentration required to inhibit 50% of cell viability, as derived from the plotted graph of percentage cell viability versus treatment concentration for each cell lines.

The percentage of cell viability was calculated using the equation:

% cell viability = ((Absorbance of treated cells – Absorbance of blank) / (Absorbance of negative control – Absorbance of blank)) × 100

2.7 Multitargeted molecular docking

2.7.1 Ligand preparation

All nine PMFs (**PMF 1** – **9**) were designed using Chemdraw Pro 8.0 (Perkin Elmer Inc, MA, USA) and saved in .mol file. Discovery Studio Visualizer v.21.1.0.20298 was used to optimize the structure using Merck Molecular Force Field (MMFF) forcefield and saved in .pdb file.

2.7.2 Protein preparation

The crystal structures of selected proteins were downloaded from the Protein Data Bank (PDB). The proteins were based on the proposed roles of PMFs in inducing cell death via multitargeted pathways. Discovery Studio Visualizer v.21.1.0.20298 was used to remove unwanted ligands and micromolecules from the retrieved protein's crystal structures. Hydrogen atoms were added to the crystallized protein structure and saved in .pdb file.

2.7.3 Molecular docking simulation

The CDocker tool from Discovery Studio Client 3.1 (Accelrys, Inc, CA, USA) was used to perform molecular docking simulations at Faculty of Pharmacy, International Islamic University of Malaysia (IIUM). The optimized parameters which include the coordinates (x,y,z) and the radius (r) were assigned to each crystallized protein structure. The binding energy was recorded and reported as -CDocker energy (kcal/mol). The ligand – protein interactions in 3-dimentional (3-D) and 2-dimentional (2-D) formats was visualized using Discovery Studio Visualizer v.21.1.0.20298.

2.7.4 Molecular docking validation

The removed co-crystallized ligands were redocked into the active sites of their respective proteins using the same optimized coordinates and radius. The redocked co-crystallized ligand was superimposed with the reference crystal complex retrieved from the Protein Data Bank using Discovery Studio Visualizer v21.1.0.20298. The root mean square deviation (RMSD) of the redocked complex was kept below the acceptable threshold of 2.00 Å to ensure the validity of the molecular docking analysis.

2.8 Density Functional Theory (DFT) Calculations

The structures of PMFs from section **2.7** were utilised for DFT analysis. BIOVIA Discovery Studio Visualizer v21.1.0.20298 was used to generate XYZ coordinate files, and input file was created using Notepad++ v8.7.7. All calculations were performed using the freely available ORCA software version 6.0.1 (Neese, 2022; Neese et al., 2020; Neese, 2011).

Previously reported protocols were followed for conducting the DFT calculations (Bakht et al., 2024; Shah et al., 2024). The Lee-Yang-Parr nonlocal correlation functional, B3LYP (Becke, 1988; Lee et al., 1988) and def2-SVP auxiliary basis set was utilized to optimize organic chemical structure of the compound under investigation (Bursch et al., 2022; Jensen, 2012). Visualization of the frontier molecular orbitals (FMOs); the highest occupied molecular orbital (HOMO) and lowest unoccupied molecular orbital (LUMO) was carried out using orca-enhanced Avogadro 1.2.0 software (Lohitha et al., 2024; Snyder & Kucukkal, 2021). The energies of the frontier molecular orbitals (E_{HOMO}, E_{LUMO}), and the energy band gap (E_{HOMO}-E_{LUMO}) were recorded and tabulated. The global chemical reactivity descriptors, such as the ionization potential (IP), chemical potential (μ), maximal charge acceptance (ΔNmax), global chemical hardness (η), global chemical softness (σ), energy change (ΔE), electrophilicity (ω), electronegativity (χ), and electron affinity (EA) were calculated using previously reported equations based on Koopmans' theory (Bhatia, 2023; Elkaeed et al., 2022).

2.9 ADMET analysis

Free online web tools were utilised to carry out the pharmacological magnitude of the selected ligands. The pharmacokinetic, drug-likeliness, and physicochemical properties of the compounds were assessed using SwissADME and ADMET Lab 2.0. Drug-likeness was evaluated based on Lipinski's Rule of Five, which states that a compound is more likely to exhibit good oral bioavailability if it has a molecular weight (MW) below 500 Da, number of hydrogen bond acceptors less than 10, number of hydrogen bond donors less than 5, calculated n-octanol-water coefficient (Clog P) less than 5.

2.10 Correlation analysis

Pearson's correlation analysis between the binding energy and the IC_{50} of the screened PMFs on both MCF-7 and MDA-MB-231 breast cancer cell lines were performed using JASP software. A positive value (> 0.800) indicates a strong positive correlation suggesting that stronger binding energy results in a lower IC_{50} of screened PMFs.

2.11 Statistical analysis

All data and results were expressed as mean ± SD and analysed using IBM SPSS Statistics version 28 (IBM Corp., Armonk, NY, USA).

3.0 Results and Discussions

3.1 PMFs isolated from K. parviflora rhizome

Identification and isolation of bioactive compounds using gravitational column chromatography from both n-hexane and chloroform fractions of *K. parviflora* extract yielded pure compounds. Elucidation and characterization of the structures of the isolated compounds, based on ^{1}H-NMR and ^{13}C-NMR analyses, confirmed the presence of nine known PMFs compounds: 5-hydroxy-3,7-dimethoxyflavone (**PMF 1**), 5-hydroxy-7-methoxyflavone (**PMF 2**), 5-hydroxy-3,7,4'-trimethoxyflavone (**PMF 3**), 5-hydroxy-7,4'-dimethoxyflavone (**PMF 4**), 5-hydroxy-3,7,3',4'-tetramethoxyflavone (**PMF 5**), 3,5,7-trimethoxyflavone (**PMF 6**), 5,7-dimethoxyflavone (**PMF 7**), 3,5,7,3',4'-pentamethoxyflavone (**PMF 8**) and 5,7,4'-trimethoxyflavone (**PMF 9**) (**Figure 1 & 2**). Functional group assignments and the corresponding ^{1}H- and ^{13}C-NMR data were visualized and tabulated in **Table 1**. Additionally, the ^{1}H- and ^{13}C- NMR spectral of isolated PMFs was also validated by comparison with previously reported studies by Ha et al. (2023), Lee et al. (2022), Luan et al. (2020), Sae-Wong et al. (2011) and Sae-Wong et al. (2009).

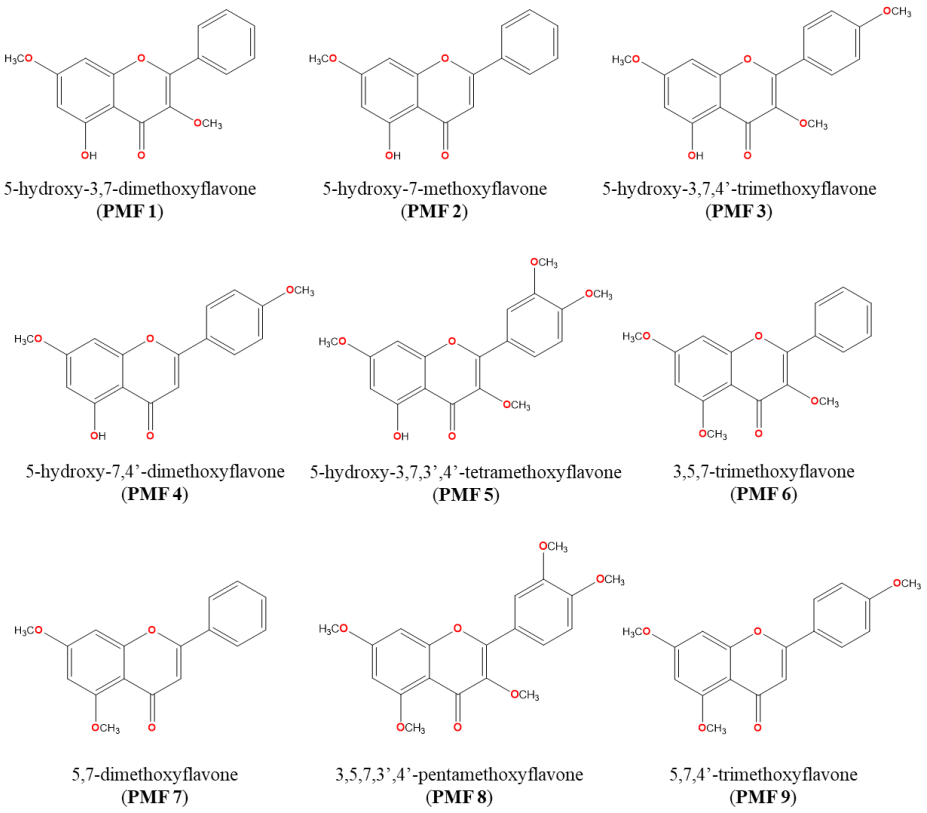

Figure 1 Structure of PMFs isolated from *K. parviflora* extract

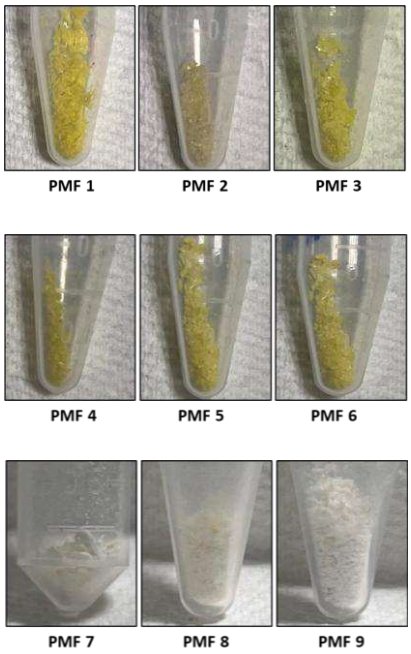

Figure 2 Physical appearance of **PMF 1** – **9** isolated from *K. parviflora* extract

:

Table 1 ^{1}H-NMR & ^{13}C-NMR spectral data of nine PMFs isolated from *K. parviflora* extract

Position	^{1}H- (mult, δ, J in Hz) & ^{13}C- (mult, δ) NMR																	
	PMF 1		PMF 2		PMF 3		PMF 4		PMF 5		PMF 6		PMF 7		PMF 8		PMF 9	
	^{1}H	^{13}C	^{1}H	^{13}C	^{1}H	^{13}C	^{1}H	^{13}C	^{1}H	^{13}C	^{1}H	^{13}C	^{1}H	^{13}C	^{1}H	^{13}C	^{1}H	^{13}C
1	-	-	-	-	-	-	-	-	-	-	-	-	-	-	-	-	-	-
2	-	156.02	-	157.84	-	156.84	-	162.15	-	155.95	-	152.73	-	159.83	-	152.01	-	160.96
3	-	139.76	6.62 (s)	105.2	-	138.94	6.56 (s)	105.5	-	139.05	-	141.88	6.57 (s)	108.51	-	140.97	6.47 (s)	107.74
4	-	179.05	-	182.57	-	178.89	-	182.49	-	178.83	-	174.27	-	175.73	-	172.47	-	175.74
5	-	162.09	-	164.05	-	162.07	-	164.05	-	162.09	-	161.05	-	160.99	-	161.02	-	162.28
6	6.35 (d, 2.2)	98.05	6.33 (d, 2.4)	98.92	6.34 (d, 2.0)	98.55	6.35 (d, 2.0)	98.73	6.35 (d, 2.0)	92.98	6.30 (d, 2.4)	96.47	6.44 (d, 2.4)	96.09	6.42 (d, 2.4)	95.59	6.44 (d, 2.0)	95.97
7	-	165.65	-	165.67	-	165.49	-	165.43	-	165.52	-	164.08	-	164.28	-	164.13	-	164.13
8	6.45 (d, 2.2)	92.3	6.45 (d, 2.0)	92.95	6.43 (d, 2.4)	92.91	6.46 (d, 2.4)	91.97	6.44 (d, 2.4)	91.63	6.48 (d, 2.0)	93.16	6.74 (d, 2.4)	93.12	6.68 (d, 2.4)	92.74	6.73 (d, 2.4)	93.09
9	-	156.99	-	162.22	-	161.76	-	162.61	-	156.79	-	158.99	-	160.07	-	158.76	-	160.17
10	-	106.27	-	106.62	-	106.12	-	103.61	-	106.11	-	109.57	-	108.99	-	109.15	-	108.89
1’	-	131.05	-	131.34	-	122.86	-	123.58	-	122.95	-	130.9	-	131.21	-	123.31	-	123.76
2’	8.05 (dd, 1.6)	128.48	7.85 (dd, 1.2)	126.1	8.05 (d, 9.2)	114.81	7.84 (d, 9.2)	128.09	7.68 (d, 2.0)	111.26	8.05 (dd, 1.6)	128.15	7.98 (dd, 2.4)	129.05	7.67 (d, 2.4)	111.49	7.92 (d, 8.8)	127.64
3’	7.51 (m)	128.71	7.5 (m)	126.1	7.00 (d, 9.2)	113.47	7.01 (d, 8.8)	115.2	-	151.42	7.48 (m)	128.15	7.53 (m)	125.93	-	149.08	7.05 (d, 9.2)	114.41
4’	7.51 (m)	130.54	7.5 (m)	131.34	-	156.09	-	157.7	-	148.79	7.48 (m)	128.26	7.53 (m)	131.67	-	151.31	-	159.77
5’	7.51 (m)	128.71	7.5 (m)	126.1	7.00 (d, 9.2)	113.47	7.01 (d, 8.8)	115.2	6.97 (d, 8.4)	110.23	7.48 (m)	128.26	7.53 (m)	125.93	7.06 (d, 8.4)	111.31	7.05 (d, 9.2)	114.41
6’	8.05 (dd)	128.48	7.85 (dd, 1.6)	126.1	8.05 (d, 9.2)	114.81	7.84 (d, 9.2)	128.09	7.74 (dd, 2.2)	122.26	8.05 (dd, 1.6)	128.15	7.98 (dd, 2.0)	129.05	7.71 (dd, 1.6)	121.52	7.92 (d, 8.8)	127.64
3-OCH_3	3.86 (s)	55.93			3.86 (s)	56.74			3.86 (s)	60.03	3.86 (s)	55.69			3.81 (s)	55.60	-	-
5- OCH_3											3.92 (s)	59.91	3.91 (s)	55.51	3.87 (s)	55.49	3.86 (s)	55.08
7- OCH_3	3.85 (s)	60.50	3.85 (s)	55.65	3.84 (s)	60.51	3.87 (s)	55.01	3.85 (s)	56.14	3.85 (s)	56.67	3.85 (s)	55.60	3.87 (s)	58.99	3.84 (s)	55.48
3’- OCH_3									3.95 (s)	56.09					3.87 (s)	55.37	-	-
4’- OCH_3					3.88 (s)	57.99	3.88 (s)	56.77	3.96 (s)	55.66					3.90 (s)	55.25	3.91 (s)	55.58
5-OH	12.58 (s)		12.69 (s)		12.65 (s)		12.80 (s)		12.63 (s)								-	-

Note: δ = chemical shift in ppm; J = coupling constant in Hz.

3.2 Cytotoxicity of nine PMFs isolated from *K. parviflora* extract on breast cancer cell lines

Preliminary cytotoxicity screening of **PMF 1** to **9** isolated from *K. parviflora* extract was conducted on two metabolically distinct breast cancer cell lines, MCF-7 and MDA-MB-231, using the MTT assay to determine the cytotoxic selectivity of the PMFs against each cancer cell line. Both breast cancer cell lines were treated with the same set of isolated compounds at concentrations ranging from 10 µM to 200 µM for up to 72-hours to determine the IC_{50} (**Figure 3**), with chemotherapy drug, doxorubicin (Dox) (0.25 - 4 µM) served as the positive control, while a non-toxic concentration of DMSO was used as the vehicle control.

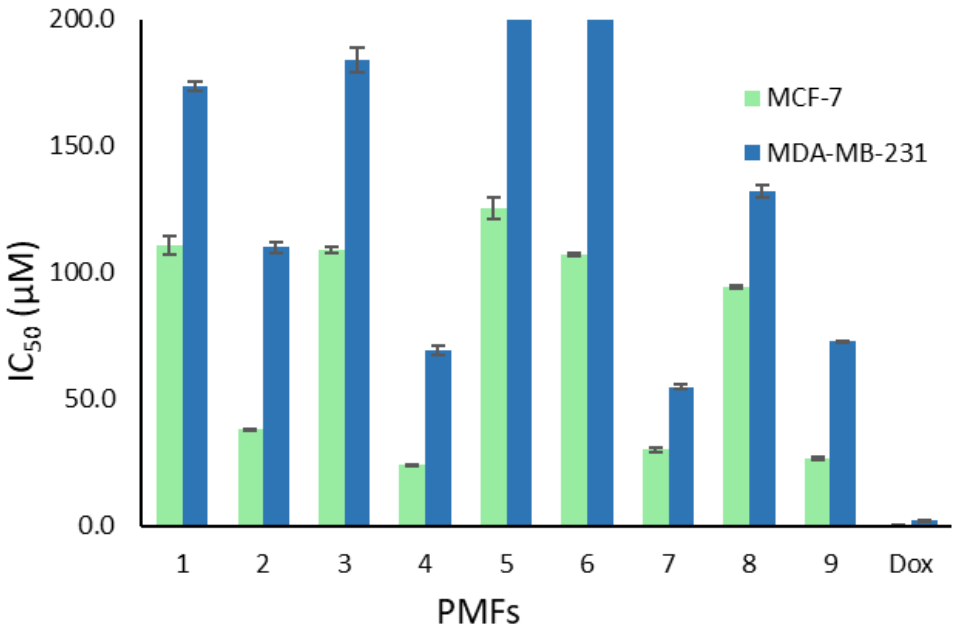

Figure 3 Cytotoxic activity of isolated PMF 1 to 9 and doxorubicin (Dox) against MCF-7 and MDA-MB-231 breast cancer cell lines after 72-hour treatment. Results are presented as IC_{50} values (µM). Data are expressed as mean ± SD (n = 3)

All nine isolated PMFs significantly induced cytotoxic effect on MCF-7 cells, with stronger inhibition than the MDA-MB-231 breast cancer cell lines after 72-hour treatment (**Figure 3**). In MCF-7 cells, all PMFs recorded IC_{50} values below 150 µM. Meanwhile, only seven PMFs exhibited IC_{50} values below 200 µM in MDA-MB-231 cells, with **PMF 5** and **6** demonstrated the weakest cytotoxic effect (IC_{50} > 200 µM). The selective cytotoxicity observed between the two breast cancer cell lines could be attributed to the phenotypic and genotypic differences. MCF-7 is a hormonal dependent call lines (estrogen and progesterone receptor-positive), on the contrary MDA-MB-231 is hormonal independent (Nohara et al., 1998). MCF-7 exhibits an epithelial phenotype with tight intercellular adhesion between the cells that contributes to the low invasiveness (Theodossiou et al., 2019; Gjerdrum et al., 2009). Additionally, the presence of estrogen and progesterone receptors mediates MCF-7 growth and reduces its aggressiveness due to sensitivity to anti-estrogen and anti-progesterone agents (Sovijit et al., 2020; Gest et al., 2013). Simultaneously, both phenotypic and hormone receptor inhibit the epithelial-mesenchymal transition (EMT) that retains the cell adhesion, low migration state and weaker aggressiveness compared to MDA-

MB-231 cell lines (Martin et al., 2013; Jiang & Mansel, 2000; Zschiesche et al., 1997). In contrast, MDA-MB-231 is a triple-negative breast cancer (TNBC) cell line, lacking hormonal receptors and exhibiting a mesenchymal phenotype, that is highly invasive and aggressive (Theodossiou et al., 2019; Gjerdrum et al., 2009). Mesenchymal cells, being loosely organized, exhibit greater migratory potential compared to epithelial cells (Franchi et al., 2020). Although invasiveness may not directly affect in-vitro cytotoxicity outcomes, the mesenchymal phenotype could contribute to the rapid proliferation rate of MDA-MB-231 cells compared to MCF-7 (Franchi et al., 2020; Parekh et al., 2018; Holliday & Speirs, 2011). The isolated PMFs compounds and doxorubicin drug as a positive control was screened for its concentration- and time-dependent cytotoxicity activity in different concentration between 10 µM up to 200 µM on MCF-7 breast cancer cell lines for 24-, 48- and 72-hour. The IC_{50} values obtained are recorded in **Table 2**. The percentage of cancer cells viability after treatments were plotted against the PMF concentration and visualized in **Figure 4**.

Table 2 IC_{50} values of isolated PMFs and doxorubicin on MCF-7 breast cancer cell lines after 24-, 48- and 72-hour treatments. Data are expressed as mean ± SD (n = 3)

Sample	compound	IC_{50} (µM ± S.D.)		
		24-hour	48-hour	72-hour
PMF 1	5-hydroxy-3,7-dimethoxyflavone	> 200	189.51 ± 3.69	110.62 ± 3.63
PMF 2	5-hydroxy-7-methoxyflavone	> 200	165.85 ± 2.33	38.20 ± 0.17
PMF 3	5-hydroxy-3,7,4'-trimethoxyflavone	> 200	> 200	108.80 ± 1.22
PMF 4	5-hydroxy-7,4'-dimethoxyflavone	155.49 ± 1.55	50.62 ± 2.21	24.12 ± 0.45
PMF 5	5-hydroxy-3,7,3',4'-tetramethoxyflavone	> 200	> 200	125.52 ± 4.30
PMF 6	3,5,7-trimethoxyflavone	> 200	> 200	106.97 ± 0.63
PMF 7	5,7-dimethoxyflavone	79.87 ± 0.70	53.12 ± 1.83	30.12 ± 0.85
PMF 8	3,5,7,3',4'-pentamethoxyflavone	> 200	170.34 ± 1.59	94.22 ± 0.70
PMF 9	5,7,4'-trimethoxyflavone	154.97 ± 1.38	94.13 ± 0.59	26.69 ± 0.81
Dox	Doxorubicin	2.37 ± 0.05	0.99 ± 0.02	0.61 ± 0.01

Note: Greater than 200 µM indicates no significant cytotoxic effect observed within the tested concentration range.

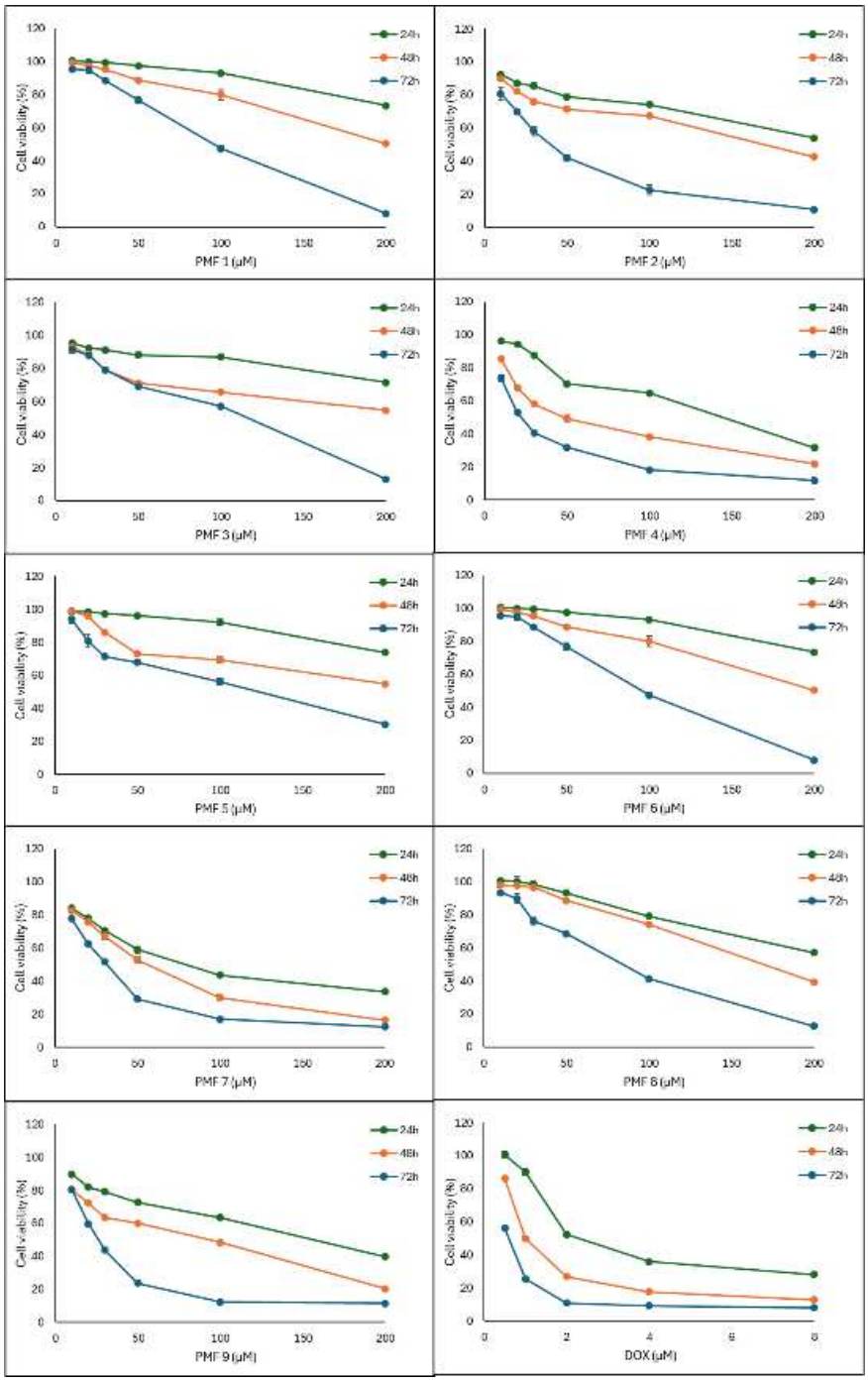

Figure 4 Cytotoxicity screening of nine isolated PMFs and doxorubicin (Dox) on MCF-7 breast cancer cell lines. Cells were treated with various concentrations (0-200 μM) of each compound for 24-, 48-, and 72-hour. Cell viability was assessed using MTT assay and plotted as percentage of viable cells. Data are presented as mean ± SD (n = 3).

The isolated **PMF 1** to **9** were screened for cytotoxic activity on MCF-7 cells at various concentrations (up to 200 μM) over 24-, 48-, and 72-hour treatment durations to determine the time- and dose-dependent effects (**Figure 4**). The increase in PMFs concentration significantly enhanced cytotoxicity while prolonged exposure correlates with stronger cell death effect in linear and logarithm relationship, resulting in stronger IC_{50} recorded. After 24-hour treatment, only **PMF 4**, **PMF 7** and **PMF 9**

demonstrated notable cytotoxicity. Longer treatment duration (48-hour) improved the anticancer effect of **PMF 1**, **PMF 2** and **PMF 8** with improved IC_{50} value. Whereas **PMF 3**, **PMF 5** and **PMF 6** achieved IC_{50} effect after 72-hour treatment. At 72-hour treatment, **PMF 4** (5-hydroxy-7,4'-dimethoxyflavone), **PMF 9** (5,7,4'-trimethoxyflavone) and **PMF 7** (5,7-dimethoxyflavone) demonstrate the strongest cytotoxic activity on the MCF-7 cell lines with IC_{50} value of 24.12 ± 0.45 μM, 26.69 ± 0.81 μM and 30.12 ± 0.85 μM, respectively. These values indicate significant reductions in cell viability comparable to the positive control, doxorubicin (Dox) (**Figure 4**). In contrast, **PMF 5** (5-hydroxy-3,7,3',4'-tretramethoxyflavone) exhibited the weakest cytotoxic effect with an IC_{50} exceeding 100 μM (125.52 ± 4.30 μM).

The toxicity of **PMF 4**, **7** and **9** were further investigated on NIH-3T3 mouse fibroblast cells, selected based on their strong cytotoxicity profile against MCF-7 breast cancer cells (**Table 3**). After 72-hour treatment, high selective cytotoxicity was observed, with **PMF 7** and **9** maintaining more than 80% cell viability when treated at their respective IC_{50} concentrations. Notably, **PMF 9** (5,7,4'-trimethoxyflavone) demonstrated the weakest toxicity with percentage of cell viability approaching 90%, indicating a favorable safety profile. However, **PMF 4** and doxorubicin showed moderate selectivity in reducing NIH-3T3 cell viability by approximately 28.41% and 22.14%, respectively at concentrations of 24.12 ± 0.45 μM and 0.61 ± 0.01 μM. Despite their potent anticancer effects, the relatively low cytotoxicity of **PMF 4**, **7** and **9** on normal fibroblast cells supports the therapeutic potential of methoxyflavone derivatives as selective anticancer agents.

Table 3 Percentage of cell viability of NIH-3T3 cells after 72-hour treatment by **PMF 4**, **7**, **9** and doxorubicin at their respective IC_{50} concentrations determined from MCF-7 breast cancer cells.

PMF	Compound name	IC_{50} on MCF-7 (μM ± S.D.)	NIH-3T3 Cell viability at IC_{50} (% ± S.D.)
4	5-hydroxy-7,4'-dimethoxyflavone	24.12 ± 0.45	77.86 ± 0.62
7	5,7-dimethoxyflavone	30.12 ± 0.85	83.43 ± 1.14
9	5,7,4'-trimethoxyflavone	26.69 ± 0.81	88.41 ± 0.48
Dox	Doxorubicin	0.61 ± 0.01	71.59 ± 0.69

3.3 Molecular docking analysis

The potent cytotoxicity observed from selected PMFs against MCF-7 cell lines suggests potential strong interaction with proteins involved in breast cancer pathogenesis. To investigate the cell death pathways, six relevant molecular targets were selected for docking: Bcl-xl (PDB: 3zk6), Bcl-2 (PDB: 4ieh), mTOR (PDB: 4drh), estrogen receptor; erα (PDB: 3ert), MMP-9 (PDB: 1gkc) and ERK2 (PDB: 6dcg) were chosen and retrieved from the Protein Data Bank (PDB). The redocking of the co-crystallized ligands to the selected proteins was utilized as a positive control in this section to preserve the docking protocol (Deb et al., 2021). The docked co-crystallized ligands were superimposed on the original retrieved ligand to evaluate the RMSD. RMSD obtained on six respective superimposed co-crystallized ligands ranging from 0.50 to 1.90 Å. Two- and three-dimensional visualization (2-D & 3-D) of the redocking protocols and amino acids involved in the interaction between ligand and protein was summarized in **Figure 5**.

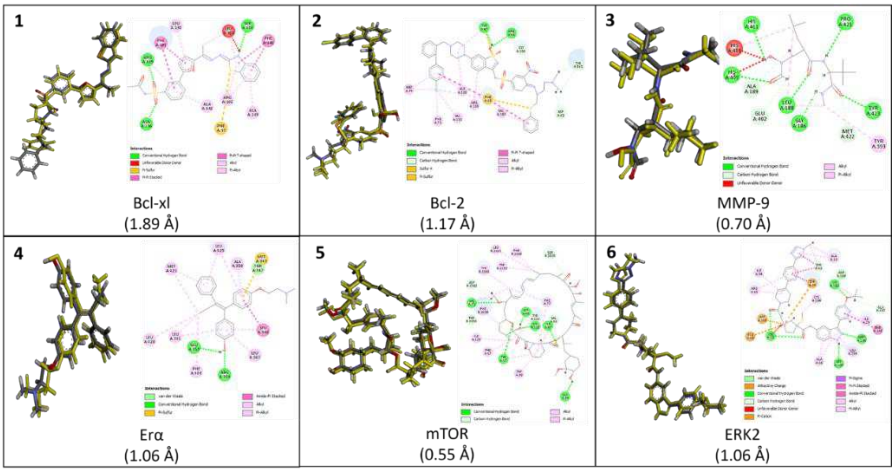

Figure 5 RMSD values and binding interaction of co-crystallized ligand with the target proteins: (1) Bcl-xL (1.89 Å), (2) Bcl-2 (1.17 Å), (3) MMP-9 (0.70 Å), (4) ERα (1.06 Å), (5) mTOR (0.55 Å), and (6) ERK2 (1.06 Å). Each panel shows the 3D superimposition of the docked pose with its original conformation (left) and the 2D interaction map (right), illustrating key binding residues. RMSD values indicate successful redocking within acceptable thresholds (RMSD < 2.0 Å), validating the docking protocol.

Redocking co-crystallized ligands with their respective protein and receptor successfully revealed the active binding pockets and interacting amino acid residues. This validation step was crucial for confirming the reliability of the docking protocol and understanding the potential interaction sites the isolated PMFs. As shown in (**Figure 5 (1)),** hydrogen bonds were formed between Bcl-xL and amino acid residues ARG139, ASN136 and SER106. In addition, several π-interactions were identified involving amino acids PHE97, PHE105, PHE146, ALA142, ARG102, ALA149 and LEU130. In **Figure 5 (2),** the interaction of co-crystallized thiadiazole-containing ligand with Bcl-2 formed hydrogen bonds through TYR67 and ARG66 amino acids residue, while GLY104, TYR161 and ASP62 amino acids participated in carbon-hydrogen bonding. Meanwhile, for MMP-9 (**Figure 5 (3)**), multiple actives amino acid residues PRO421, TYR423, GLY186, LEU188, HIS405 and HIS411 engaged in strong hydrogen bonding, with the ligand dominated as the hydrogen bond acceptor. In **Figure 5 (4)**, 4-hydroxytamoxifen (co-crystallized ligand extracted from ERα) formed strong hydrogen bond with GLU353 and ARG394 amino acids. Meanwhile, redocking of rapamycin into the mTOR protein (**Figure 5 (5)**) revealed strong hydrogen bond interactions with HIS71, ASP68, LYS121, ILE87, TYR57 and GLY84 within the active binding pocket. Lastly, the ERK2 inhibitor (**Figure 5 (6)**) formed hydrogen bonds with LYS112, MET106, ASP104 and LYS52, and displayed massive π-interactions involving more than ten surrounding residues.

3.4 Molecular docking of PMFs with target proteins

The nine isolated PMFs were designed, structurally optimized and docked into the defined binding sites of the selected proteins and receptors based on the validated docking parameters obtained in section **3.3**. Molecular docking was conducted using the CDocker algorithm which assesses the binding energy between the PMFs and respective protein and receptor. The scoring of CDocker energy represents the strength of ligand-protein interaction which includes the internal ligand strain (Deb et al., 2021). The CDocker binding energy of each PMF on respective protein was clustered based on different PMF

compound (**Figure 6**). Based on Figure 4.30, analysis of the Cdocker binding energy grouped by each PMF provides interesting insights. PMFs demonstrates the strongest binding interaction with ERK2, followed by the estrogen receptor and MMP-9. ERK2, a major MAPK downstream marker, regulator for cancer cell apoptosis and autophagy recorded the highest CDocker binding energy with all PMFs compound, except for **PMF 1** (erα). The distinct in CDocker binding energy of the PMFs compound on each protein illustrates the unique behaviour of the PMFs targeted to different protein markers. The position of amino acids within the binding pocket of protein plays a huge role in activating strong binding interaction with the PMFs.

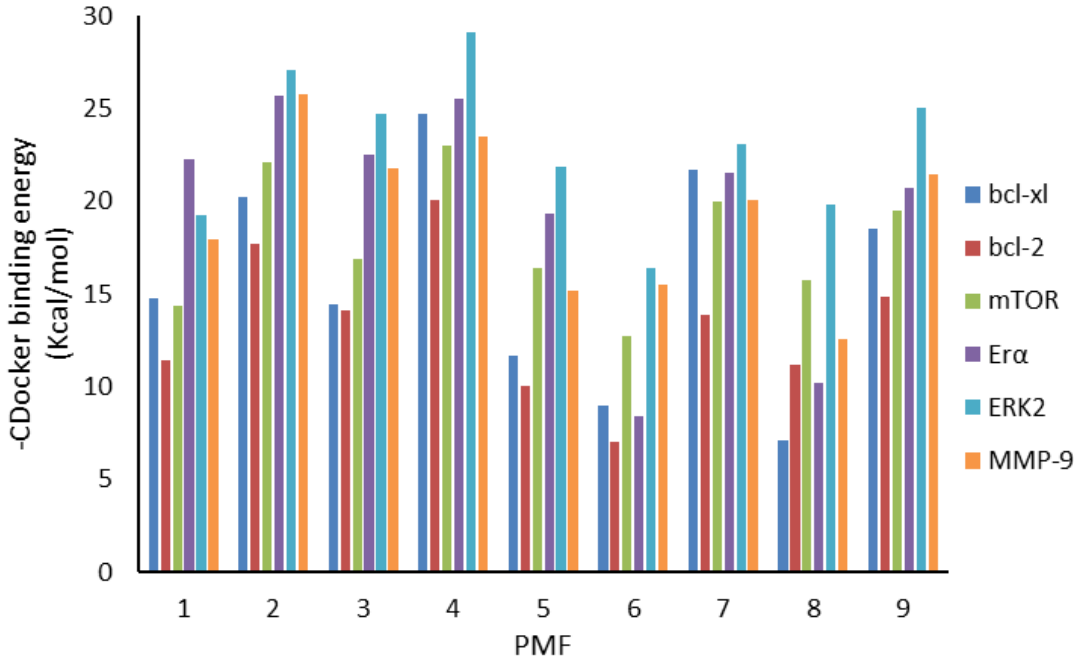

Figure 6 The comparison of -CDocker binding energy score clustered by PMFs

3.4.1 Binding interaction between PMFs and bcl-xl protein (PDB: 3zk6)

The molecular docking of **PMF 4** with Bcl-xl generates the strongest binding energy (-24.73 Kcal/mol) (**Figure 7**). The stabilization of **PMF 4** pharmacophore was achieved with well-fitted binding posed, sandwiched between the PHE105 and ARG139 amino acids residues. The amino acids interaction comprises of intramolecular hydrogen bonding between the C5-OH and the carbonyl group (1.94 Å), supplemented with two hydrogen bonds between ARG139 and the carbonyl group (2.24 & 2.70 Å). **PMF 7** binding energy scores however was lower than **PMF 4** despite generated four hydrogen bonds with ARG139, each two bonds arise from C5-OCH_3 (2.11 & 2.92 Å) and the carbonyl group (2.62 & 3.06 Å), respectively based on **Figure S21** in supplementary materials. The oxygen atom bonded to the methyl group in **PMF 7** reduced the electron density on oxygen atom, led to a weaker binding strength compared to similar interaction with the carbonyl moieties as in **PMF 4** (Siewert et al., 2022; Ramanadham et al., 1993). The presence of hydrogen bond interactions on C5-OCH_3 shifted the orientation of hydrogen bond formed with the carbonyl group resulted in greater bond length, leading to overall weaker binding energy of **PMF 7** (Fargher et al., 2022; McREE, 1999). **PMF 6** and **8** reported the weakest binding energy (-9.01 & -7.12 Kcal/mol) due to limited hydrogen bonding formation. The absence of intramolecular hydrogen bonding of C5-OH and weaker hydrogen bond interaction between

C9-O1-C2 ether group and ARG139 exposed greater ligand constraint that reduced the binding affinity (Whaley et al., 2013). Additionally, the 3-D visualization on **Figure 7 (B)** highlights the presence of C3-OCH_3 on **PMF 8** and disrupts the highly tight binding pocket which altered the optimum binding pose when compared to **PMF 4**. Consequently, all PMFs with C3-OCH_3 group (**PMF 1**, **3**, **5**, **6** & **8**) observed a reduction in binding strength with bcl-xl as the hydrogen bond interactions were substituted with weaker carbon-hydrogen intramolecular interaction with the carbonyl group (**Figure S21**). The intramolecular interaction and steric effect of C3-OCH_3 may induce a conformational adjustment, influencing the positioning of ARG139 to favor hydrogen bonding with the ether group (C9-O1-C2) and hindered hydrogen bond formation with the carbonyl group, as observed in **PMF 2**, **4**, **7** and **9**.

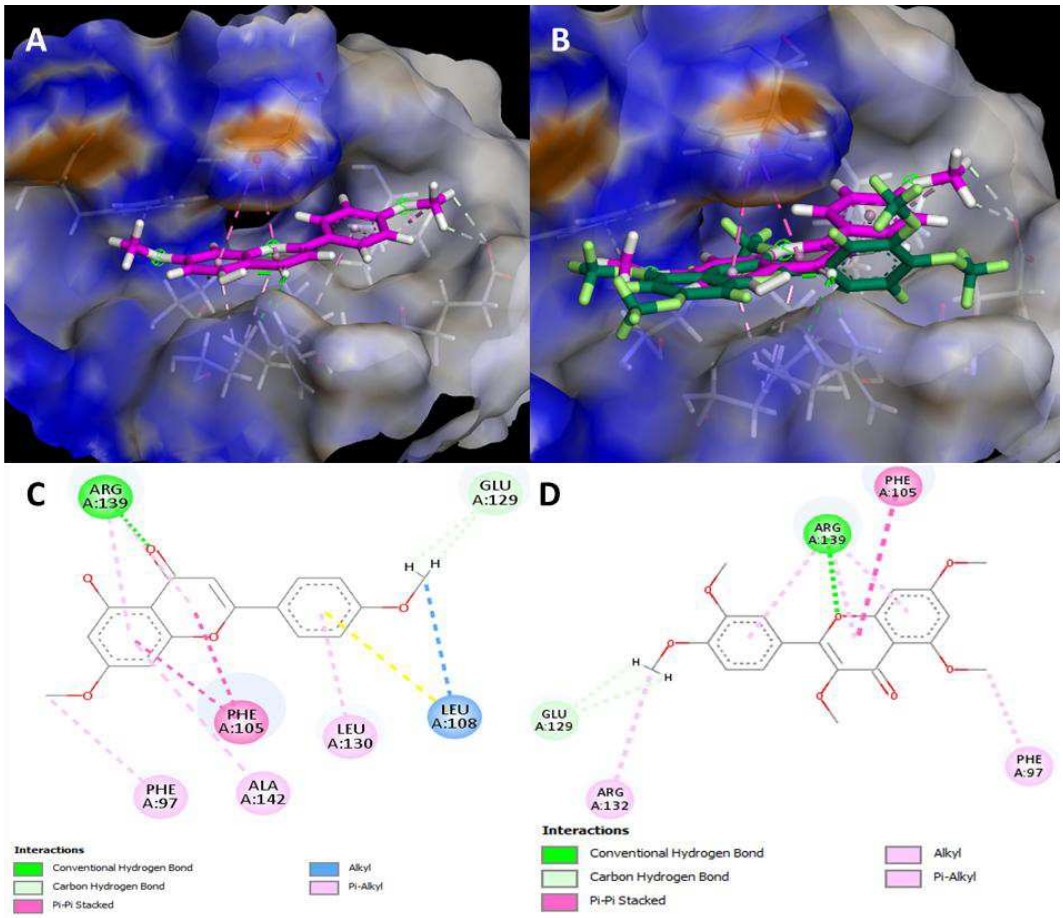

Figure 7 3-D ligand-protein interaction of (A) **PMF 4** with Bcl-xl; (B) comparison between binding pose of **PMF 4** (pink) with the highest binding energy and **PMF 8** (green); which yielded the weakest binding energy with Bcl-xl protein; 2-D ligand-protein interaction of (C) PMF 4 and (D) PMF 8 with Bcl-xl protein.

3.4.2 Binding interaction between PMFs and mTOR protein (PDB: 4drh)

Both **PMF 2** and **4** established the strongest, albeit comparable CDocker binding energy (-22.15 & -22.97 Kcal/mol) with unique interaction. The strong binding effect of **PMF 2** was secured by hydrogen bonding between oxygen atoms of C7-OCH_3 with amino acid HIS71 (2.89 Å). Meanwhile, amino acid ILE87 initiates a strong hydrogen bond with the oxygen atom of C5-OH (3.09 Å) in **PMF 4**. Both HIS71 and ILE87 were active amino acids in redocking of mTOR protein with the co-ligand, tamoxifen (**Figure 8**). Pharmacophore changes shifted the PMF orientation within the binding pocket of mTOR protein that

hindered specific target of amino acids to the favorable functional group in PMFs. For instance, HIS71 assists in strong hydrogen bonding with oxygen atom of C7-OCH_3 in **PMF 9** (-19.50 Kcal/mol). Meanwhile, the interaction of ILE87 with the C7-OCH_3 instead of C5-OH leads to weaker binding strength of **PMF 3** (-16.87 Kcal/mol), **5** (-16.37 Kcal/mol) and **8** (-15.72 Kcal/mol). Interestingly, **PMF 7** established strong interaction with the mTOR protein (-19.99 Kcal/mol) through π-interactions and carbon-hydrogen bonding, with the absence of hydrogen bonding. The carbon donor in hydrogen bonds was significantly weaker compared to the conventional hydrogen bond between N–H---O, nevertheless stronger than the π-interactions (Nanda & Schmiedekamp, 2007).

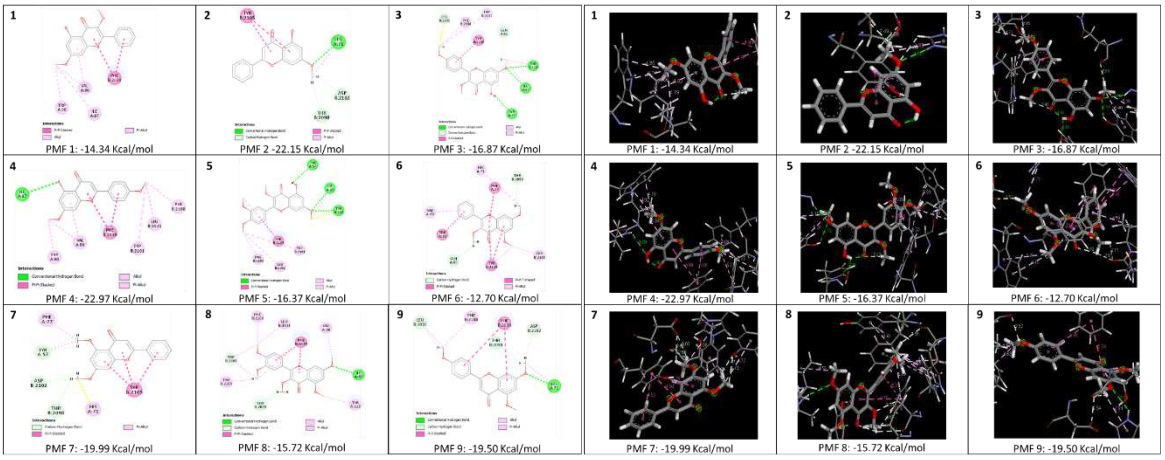

Figure 8 2-D & 3-D ligand-protein interaction between PMF 1 to 9 with mTOR protein

3.4.3 Binding interaction between PMFs and bcl-2 protein (PDB: 4ieh)

The PMFs recorded strong binding energy with bcl-2, however lower when compared to bcl-xl and mTOR (**Figure 9**). Both **PMF 4** (-20.10 Kcal/mol) and **PMF 2** (-17.72 Kcal/mol) displayed strong binding effects, assisted by hydrogen bonding between the C5-OH and GLY104 and ARG105, the active amino acids in the binding site of bcl-2 protein (**Figure 5**). The absence of hydrogen bonding weakens the binding energy of **PMF 9** and **7** (-14.89 & -13.83 Kcal/mol), nevertheless superior compared to the rest of PMF, anchored by the noncovalent π-π T-shape interactions with amino acid TYR161 (Table 4.16). Although the π-interaction was reportedly weak, the π-π T-shape or commonly known as edge-to-face stacked, was the strongest among the class of π-interactions within the aromatic group (Zhuang et al., 2018). The lack of both hydrogen bond and π interactions leads to **PMF 6** yielding the weakest binding energy (-7.04 Kcal/mol). Interestingly, **PMF 3** (-14.10 Kcal/mol), **PMF 5** (-10.01 Kcal/mol) and **PMF 8** (-11.19 Kcal/mol) displayed weak binding energy despite multiple hydrogen bonding with the active site. For instance, **PMF 8** formed six hydrogen bonding between ARG66 and the C3'- and C4'-OCH_3. Meanwhile, the active amino acid ARG105 formed the hydrogen bonds with the carbonyl group and C5-OH. Nevertheless, the amino acids that are associated with multiple hydrogen bonding with the PMF do not participate in molecular interaction with the co-crystallized ligand (Figure 4.29), that justifies unexpected weaker binding score.

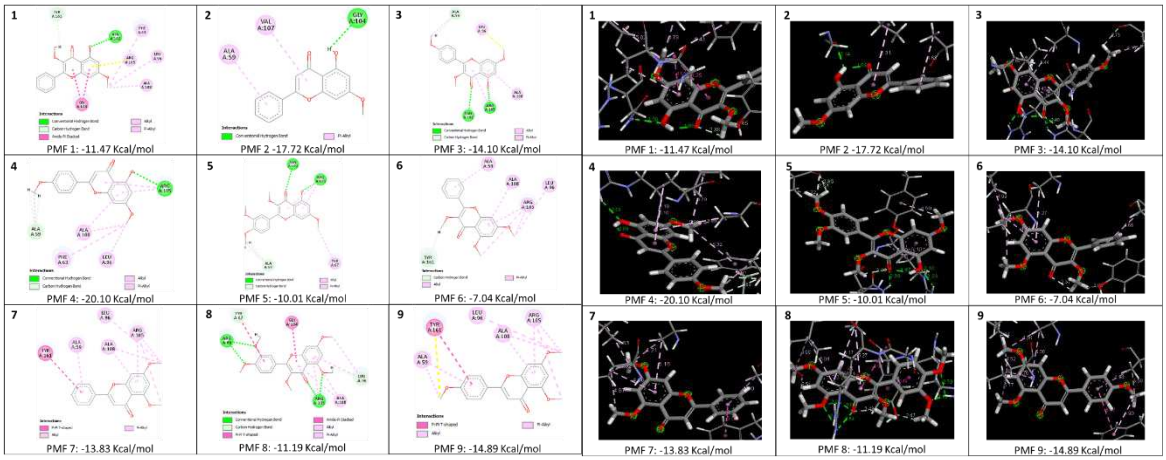

Figure 9 2-D & 3-D ligand-protein interaction between PMF 1 to 9 with bcl-2 protein

3.4.4 Binding interaction between PMFs and estrogen, er*α* receptror (PDB: 3ert)

The docking between PMFs and the estrogen receptor revealed unique interactions that lead to strong binding energy reported on **PMF 1** to **5** having C5-OH, and **PMF 7** and **9** for C5-OCH_3. Based on the 2-D and 3-D visualization in **Figure 10**, the interaction of MET343 with the aromatic ring B flavone in π-sulfur interaction significantly increases the binding strength. MET343 was an active amino acid that involved interaction with the co-crystallized ligand on similar receptors. Interestingly, the MET343 only exists and interacts with the aromatic ring B with hydroxylated PMF. The intramolecular hydrogen bonding between C5-OH and carbonyl group hindered potential amino acid interaction on the C5 position. Thus, the C5-OCH_3 PMFs open potential hydrophobic interaction, that rearranges the conformation of PMF within the binding pocket. As a result, the binding strength of **PMF 7** and **9** was dominated by carbon-hydrogen bonding by C7-OCH_3. Meanwhile, **PMF 6** and **8** reported the weakest binding strength due to π-sulfur interaction with the unfavorable ring C conjugated ring.

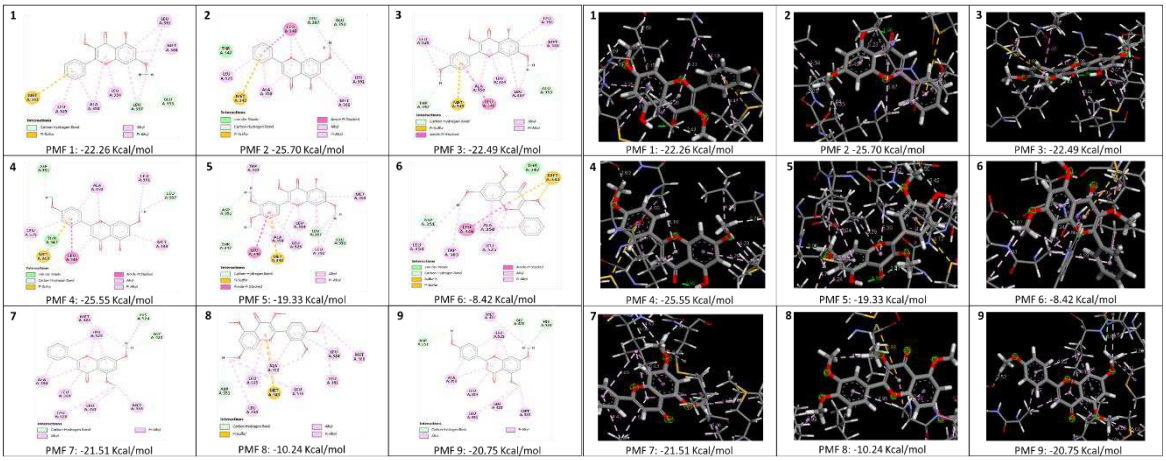

Figure 10 2-D & 3-D ligand-protein interaction between PMF 1 to 9 with estrogen receptor, er***α***.

3.4.5 Binding interaction between PMFs and MMP-9 protein (PDB: 1gkc)

The protein-ligand interaction between PMFs and MMP-9 protein associated with hydrogen bonding formation between amino acid and the carbonyl group and ether group (**Figure 11**). For instance, the active amino acid residue LEU188 and ALA189 initiate strong hydrogen bonding with the carbonyl group of **PMF 2** and **4**, leads to stronger binding effect. The formation of weak intramolecular interaction between C3-OCH_3 and the carbonyl group affecting the binding strength for **PMF 1**, **3**, **5**, **6** and **8**. The methyl group hindered additional hydrogen bonding to the carbonyl group, leads to greater bond distance and weaken the binding energy. Additionally, the C5-OH interaction with the ALA189 could disrupt the interaction with C4=O of **PMF 1** with ALA189, that reduce the binding strength. Meanwhile, unexpected higher binding strength for **PMF 3** attributed to the interaction of HIS401 with the O1 ether group. The interaction of PMF 7 and 9 were controlled by hydrophobic interactions supported by hydrogen bonding between TYR423 and the carbonyl group and C5-OCH_3 of **PMF 9**.

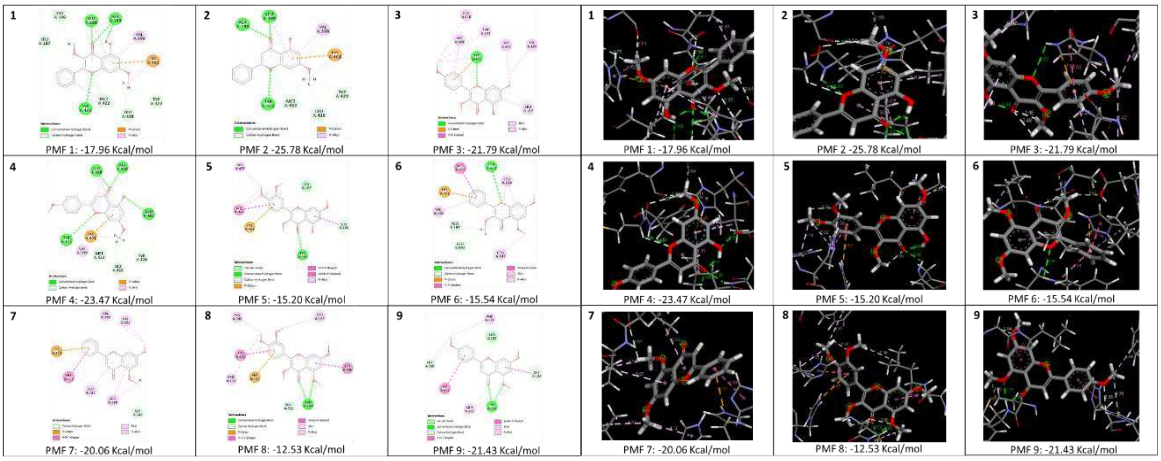

Figure 11 2-D & 3-D ligand-protein interaction between PMF 1 to 9 with MMP-9 protein.

3.4.6 Binding interaction between PMFs and ERK2 protein (PDB: 6dcg)

As mentioned previously, the stabilization of PMFs by the C5-OH group contribute to greater binding strength of **PMF 1** to **5**. The presence of C4'-OCH_3 further elevated the binding energy of **PMF 4** (-29.15 Kcal/mol), based on 2-D and 3-D visualization on **Figure 12**. As the source of strong hydrogen bonding was shifted to ring B, the unfavourable effect of C3-OCH_3 was minimized, which lead to the unexpected higher binding energy of **PMF 3** (-24.72 Kcal/mol). Nevertheless, the absence of C4'-OCH_3 was replaced by strong interaction of C4 carbonyl group with LYS52, thus retained the strong binding energy of **PMF 2** (-27.10 Kcal/mol). The absence of both condition lead to the weaker binding strength of **PMF 1** (-19.29 Kcal/mol). Similar trend was also observed for **PMF 6** to **9**. **PMF 9** achieved the strongest binding energy attributed to strong interaction of C4'-OCH_3 with amino acid THR66 (BE: -25.04 Kcal/mol). Similarly, the LYS52 amino acid residue dominated the hydrogen bonding interaction with the carbonyl group of **PMF 7** (-23.07 Kcal/mol), retained strong binding energy. Unexpectedly the presence of neighbouring C3'-OCH_3 for both **PMF 5** and **8** leads to the rearrangement of the PMFs orientation and failed to attract LYS52, leads to lower binding strength for both compounds. Lastly, **PMF 6** demonstrated the weakest binding energy, due to the presence of unfavored C3-OCH_3, the absence of C5-OH and C4'-OCH_3, and lack of hydrogen bonding interaction initiated by the active amino acid LYS52 on ring B.

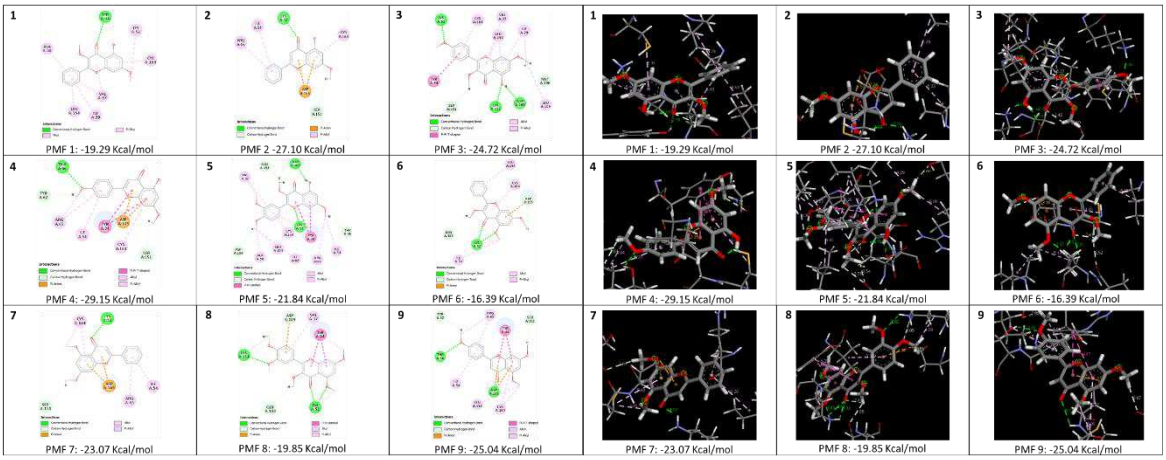

Figure 12 2-D & 3-D ligand-protein interaction between PMF 1 to 9 with ERK2 protein.

3.5 Density-Functional theory (DFT) analysis

The DFT is an ab initio quantum-mechanical computational tool that is useful in various fields of research, vitally in drug design and discovery in investigating the electronic properties of the atoms, molecules and compounds (Bakht et al., 2024). DFT calculates the ground-state energy by solving the Kohn–Sham equations, using electron density as the central variable rather than the many-electron wavefunction used in traditional quantum mechanical methods (Shakerzadeh, 2016). In this study, the DFT calculation was carried out at the B3LYP/def2-SVP theory level to optimize the structures of PMFs (Lohitha et al., 2024). The optimized frontier molecular orbitals (FMO); highest occupied molecular orbitals (HOMO), lowest unoccupied molecular orbitals (LUMO) and the HOMO-LUMO energy gap (ΔE) was visualized in **Figure 13** and **14**. Meanwhile, the calculated global reactivity descriptors were derived from Koopman's approximation, which includes ionization potential (IP), electron affinity (EA), electronegativity (χ), chemical potential (μ), chemical hardness (η), chemical softness (σ), electrophilicity index (ω) was tabulated in **Table 4**.

Frontier molecular orbitals (FMO), comprises of HOMO and LUMO were crucial to determine the chemical reactivity and electronic properties of PMFs (Bakale et al., 2023; Elkaeed et al., 2022). The energy difference between HOMO to LUMO, denoted as ΔE indicates the energy required for excitation or transfer of electron within the FMO (Bakht et al., 2024). Based on **Figure 13** and **14**, **PMF 2** demonstrated the lowest HOMO and LUMO energy levels (E_{HOMO} = -6.058 eV; E_{LUMO} = -2.037 eV). Generally, higher energy levels in HOMO (less negative) increased the electron-donor potential as electron was held less tightly within the compound, whereas lower energy levels in LUMO (more negative) elevate the electrophilicity effect in attracting electrons (Shah et al., 2024). Meanwhile, **PMF 5** yielded the smallest energy gap, ΔE = 3.842 eV; nevertheless, was significantly higher compared to the commercial drug, doxorubicin (ΔE = 2.838 eV). The sequence of PMFs' energy gaps from the lowest to highest as follows: **PMF 5** < **PMF 1** < **PMF 3** < **PMF 8** < **PMF 2** < **PMF 4 < PMF 6** < **PMF 7** < **PMF 9**. The smaller HOMO-LUMO energy gap indicates greater reactivity with low kinetic stability, meanwhile greater energy gap contributes to greater stability and less reactivity (Akl et al., 2025). Computed DFT screening confirmed the stability of PMFs, particularly **PMF 4**, **7** and **9** which are relatively more stable and less reactive. Thus, the strong cytotoxicity of these PMFs indicates the specificity and favorability between the PMFs structure to the binding pocket of protein targets, compared to the more reactive PMFs (PMF 5 and 1) that demonstrate weaker binding strength and toxicity effect on breast cancer cell lines.

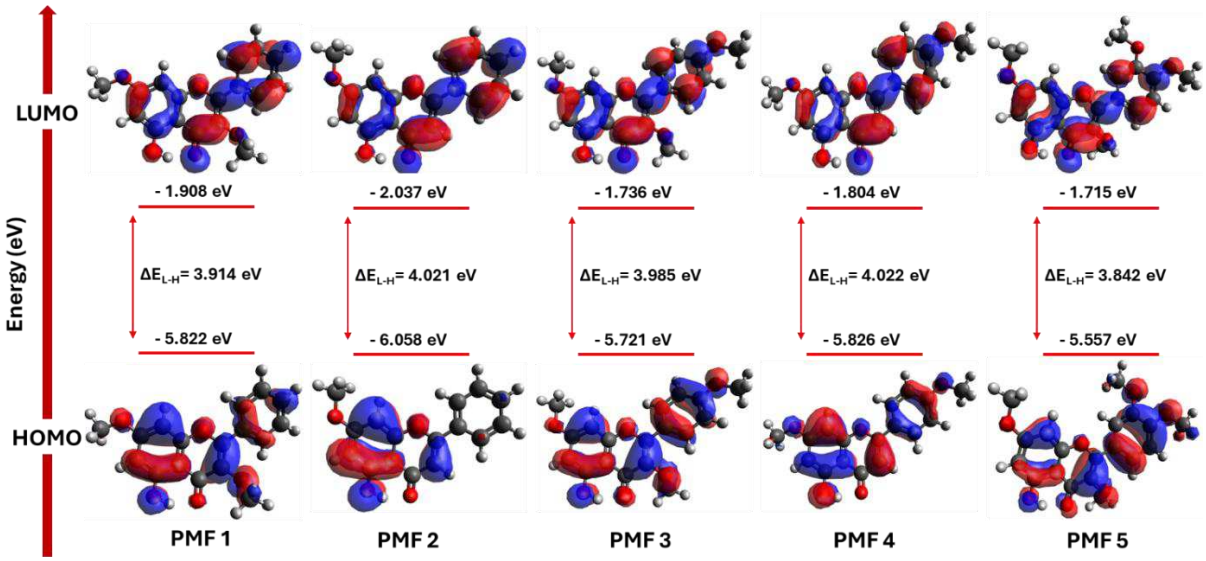

Figure 13 Representations of optimized structures, HOMO and LUMO orbitals visualization and the energy gap, ΔE of **PMF 1** to **5**

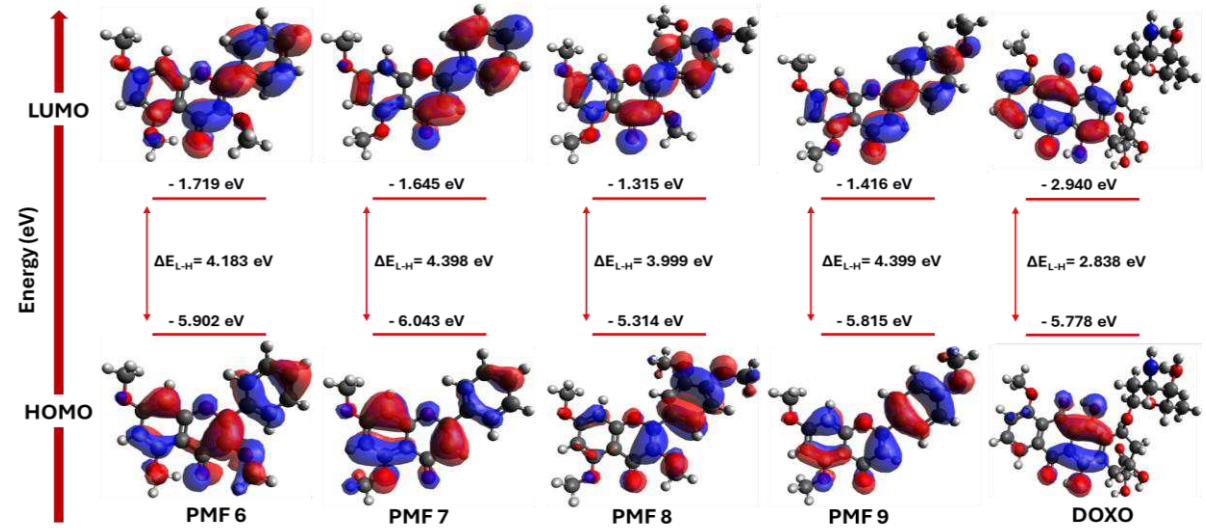

Figure 14 Representations of optimized structures, HOMO and LUMO orbitals visualization and the energy gap, ΔE of **PMF 6** to **9** and doxorubicin drug.

The electron delocalization in HOMO and LUMO were symmetrically positioned on both aromatic ring A and B, based on **Figure 13** and **14.** The vast area of the electron-rich region assists in stabilizing the compound with greater delocalization (Bakht et al., 2024; Ahmad et al., 2023). Based on both respective figures, larger HOMO orbitals lobes were observed on chromone ring A compared to phenyl ring B, which signifies the nucleophilic sites of the PMFs. Nevertheless, several exceptions were observed for **PMF 2** and **8**. On **PMF 2**, the electron-rich region was highly concentrated only on aromatic ring A, meanwhile for **PMF 8**, the nucleophilic site accumulated on aromatic ring B. In LUMO, all PMFs observed larger lobes on ring B, with smaller lobes on aromatic ring A and aliphatic ring C, indicates the electron deficient region. Additionally, the electrophilic region of C4 carbonyl group and ether group

(C9-O1-C2) from LUMO further validates the electron-acceptor roles of both functional groups as observed in the molecular docking section.

The global reactivity descriptors were calculated based on DFT analysis using Koopman's approximation, summarized in **Table 4**. As the HOMO-LUMO energy gap demonstrates the reactivity of the compounds, the calculated reactivity descriptors could describe the electronic properties of the isolated compounds. Based on the formula described, the electron affinities and the ionization potential influence the ability to attract or donate electrons. Elevated electron affinity, EA generally correlated with the elevated electrophilicity index, reduced chemical potential and its electronegativity. The chemical potential (μ) values ranged from −4.048 to −3.615 eV, reflecting the compounds' tendency to lose electrons. More negative μ implies higher electron-donating ability. For example, **PMF 2** yielded the lowest μ (−4.048 eV), consistent with its high electronegativity (χ = 4.048 eV) and electrophilicity index (ω = 4.074), suggesting strong electron-accepting potential (Von Szentpály et al., 2020). Meanwhile, the chemical hardness was inversely proportional to the chemical softness, correlating with molecular flexibility and polarizability. Doxorubicin, the reference drug, showed the highest softness (σ = 0.705) compared to PMFs, which generally exhibited lower softness and electrophilicity, implying more selective or targeted interactions (LoPachin et al., 2019; LoPachin & Gavin, 2015). Overall, the electronic descriptors suggest that **PMF 2** and **4** possess favorable stability and moderate electrophilicity, while **PMF 8** is comparatively more reactive and unstable that may be influenced particularly in ligand–target interactions. Interestingly, the electrophilicity index of doxorubicin (ω = 6.695) far exceeds those of the PMFs, consistent with its broad-spectrum cytotoxicity and aggressive reactivity profile of the commercial drug. These findings underscore the relevance of HOMO–LUMO descriptors and Koopmans-derived parameters in rationalizing and predicting bioactivity trends, further supported by IC_{50} and docking correlation data.

Table 4 Global reactivity descriptors of PMF 1-10 and doxorubicin drug based on Koopman's approximation

PMF	E_{HOMO} (eV)	E_{LUMO} (eV)	IP	EA	ΔE (eV)	μ	η	σ	χ	ω
1	-5.822	-1.908	5.822	1.908	3.914	-3.865	1.957	0.511	3.865	3.817
2	-6.058	-2.037	6.058	2.037	4.021	-4.048	2.011	0.497	4.048	4.074
3	-5.721	-1.736	5.721	1.736	3.985	-3.729	1.993	0.502	3.729	3.489
4	-5.826	-1.804	5.826	1.804	4.022	-3.815	2.011	0.497	3.815	3.619
5	-5.557	-1.715	5.557	1.715	3.842	-3.636	1.921	0.521	3.636	3.441
6	-5.902	-1.719	5.902	1.719	4.183	-3.811	2.092	0.478	3.811	3.471
7	-6.043	-1.645	6.043	1.645	4.398	-3.844	2.199	0.4548	3.844	3.360
8	-5.314	-1.315	5.314	1.315	3.999	-3.315	2.000	0.500	3.315	2.747
9	-5.815	-1.416	5.815	1.416	4.399	-3.616	2.200	0.4546	3.616	2.972
Doxo	-5.778	-2.940	5.778	2.940	2.838	-4.359	1.419	0.705	4.359	6.695

3.6 Drug likeness and ADMET evaluation

Drug-likeness of a compound was evaluated by the similarities of its physicochemical properties to a known sets of drugs to predetermine the potential use in clinical trials. Lipinski's rule of five is a common strategy used in preliminary drug-likeness evaluation, where the compound was screened to ensure the parameters set within the acceptable threshold to the physicochemical properties of a drugs

(Zhu et al., 2023). Whereas ADMET (Absorption, Distribution, Metabolism, Excretion and Toxicity) screening further elucidates how a drug candidate interacts with the body, influencing its potential for success in development. Specifically, ADMET evaluations assist in determining the absorption properties, distribution specificity, metabolism parameters and excretion efficiency, and if it poses unacceptable toxicity risks. The pre-screening of ADME on compound significantly reduced the degree of pharmacokinetics-related failure in the clinical phase (Afridi et al., 2024; Daina et al., 2017).

The drug-likeness and ADMET properties of **PMF 1** to **9** were evaluated using free available software tools SwissADME and ADMETlab2.0. The drug-likeness properties of **PMF 1** to **9** were tabulated in **Table 5**. The screening reaffirmed that all PMFs do not violate the Lipinski rule of five. As previously mentioned in molecular docking and DFT analysis, the PMFs interaction and strong toxicity attributed to its properties of having multiple HBA sites, with only PMF 1 to 5 having at least one HBD capacity. The Topological Polar Surface Area (TPSA), molar refractivity (MR) and consensus Log Po/w are relatively moderate for **PMF 1** to **9**, with exception to lipophilicity index of **PMF 6** to **9** that demonstrate a minor increase due to the absence of hydroxy group. Nevertheless, all PMFs were potentially absorbed in the gastrointestinal (GI) tract effectively after oral administration. **Table 5** also indicates favorable synthetic accessibility (SA) score for **PMF 1** to **9** thus could be easily synthesized. The favorable drug-likeness properties of the PMFs were further validated by ADMET computational screening using ADMETlab2.0 (**Table 6**). **Table 6 (A)** confirmed the absorption and distribution properties of PMFs. All PMFs show greater potential as P-glycoprotein (P-gp) inhibitor and were highly permeable to cell membrane based on the caco-2 permeability index, an indicator used to assess the absorption of compound in the human GI system (Mahmoodi et al., 2024). The favorable human intestinal absorption HIA value, plasma protein binding (PPB) exceeds 90% and low blood-brain barrier index indicates greater bioavailability and safety profile of the PMFs. Additionally, all PMFs demonstrated strong inhibitor on CYP3A4 and CYP2C19 enzymes, thus unlikely to metabolize, compared to other class of enzymes. Detailed analysis on the toxicity and elimination parameters could be obtaine don **Table 6 (C)** and **(D)**, as in general, all PMFs demonstrated low carcinogenicity and non-toxic, with exception to **PMF 7** that also demonstrate higher AMES toxicity. Overall, the drug-likeness and ADMET screening validate the safety profile of **PMF 1** to **9** with greater bioavailability despite several PMFs showing high lipophilic properties. Nevertheless, computational screening may also highlight its limitation in examining the hydrogen bond donor (HBD) availability of the PMFs, given the rises of intramolecular hydroen bonding (IHB) that limit the role of HBD specifically in **PMF 1** to **5**, as discussed in in-vitro, and molecular docking section.

Table 5 Drug-likeness properties of **PMF 1** to **9**

PMF	MW (g/mol)	HBA	HBD	TPSA (Å2)	Consensus Log $P_{o/w}$	MR	GI Absorption	Lipinski	Bioavailability Score	PAINS (alert)	SA score
1	298.29	5	1	68.9	2.89	82.93	High	0	0.55	0	3.32
2	268.26	4	1	59.67	2.95	76.43	High	0	0.55	0	3.01
3	328.32	6	1	78.13	2.89	89.42	High	0	0.55	0	3.45
4	298.29	5	1	68.9	2.79	82.93	High	0	0.55	0	3.14
5	358.34	7	1	87.36	2.86	95.91	High	0	0.55	0	3.64
6	312.32	5	0	57.9	3.05	87.4	High	0	0.55	0	3.45
7	282.29	4	0	48.67	3.13	80.9	High	0	0.55	0	3.15
8	372.37	7	0	76.36	3.04	100.4	High	0	0.55	0	3.78

9	312.32	5	0	57.9	3.1	87.4	High	0	0.55	0	3.28

Table 6 ADMET profile of **PMF 1** to **9**. (A) absorption and distribution parameters, (B) Metabolism parameters, (C) Elimination parameters and (D) Toxicity parameters.

A) Absorption and Distribution

PMF	Caco-2 permeability	Pgp-Inhibitor	Pgp-substrate	HIA (%)	PPB (%)	Volume of distribution (L/Kg)	BBB
1	-4.795	+++ 0.998	--- 0.001	--- 0.006	94.48	0.666	--- 0.035
2	-4.824	+ 0.665	- 0.434	--- 0.008	96.91	0.599	--- 0.046
3	-4.692	+++ 0.998	--- 0.000	--- 0.007	89.39	0.798	--- 0.021
4	-4.738	++ 0.829	--- 0.009	--- 0.009	93.66	0.723	--- 0.031
5	-4.704	+++ 0.998	--- 0.001	--- 0.009	81.55	0.86	--- 0.019
6	-4.687	+++ 1.000	--- 0.000	--- 0.005	84.91	0.864	-- 0.102
7	-4.719	+++ 0.998	--- 0.008	--- 0.006	90.72	0.827	--- 0.1
8	-4.66	+++ 1.000	--- 0.001	--- 0.007	71.37	0.955	--- 0.096
9	**-4.654**	+++ 0.999	--- 0.002	--- 0.007	84.12	0.918	--- 0.094

B) Metabolism

PMF	CYP1A2 inhibitor	CYP1A2 Substrate	CYP3A4 inhibitor	CYP3A4 Substrate	CYP2C9 inhibitor	CYP2C9 Substrate	CYP2C19 inhibitor	CYP2C19 Substrate	CYP2D6 inhibitor	CYP2D6 Substrate
1	+++ 0.971	+++ 0.925	+ 0.673	-- 0.182	++ 0.849	+++ 0.921	+++ 0.924	-- 0.157	++ 0.712	++ 0.857
2	+++ 0.986	++ 0.883	+ 0.685	-- 0.167	++ 0.82	+++ 0.925	+++ 0.924	--- 0.084	++ 0.755	++ 0.898
3	+++ 0.953	+++ 0.954	++ 0.735	-- 0.281	++ 0.83	+++ 0.942	++ 0.886	-- 0.201	+ 0.614	+++ 0.923
4	+++ 0.976	+++ 0.949	++ 0.77	-- 0.272	++ 0.819	+++ 0.942	++ 0.85	--- 0.098	++ 0.708	+++ 0.935
5	++ 0.873	+++ 0.974	++ 0.756	- 0.427	+ 0.699	+++ 0.925	++ 0.744	+ 0.601	- 0.381	+++ 0.926
6	+++ 0.938	+++ 0.962	++ 0.779	-- 0.286	++ 0.867	+++ 0.922	+++ 0.943	- 0.451	- 0.491	+++ 0.908
7	+++ 0.979	+++ 0.956	++ 0.763	-- 0.237	++ 0.851	+++ 0.923	+++ 0.948	-- 0.212	+ 0.517	+++ 0.921
8	+ 0.618	+++ 0.981	++ 0.813	+ 0.571	++ 0.682	+++ 0.925	++ 0.737	++ 0.867	--- 0.08	+++ 0.941
9	+++ 0.954	+++ 0.965	++ 0.82	- 0.431	++ 0.831	+++ 0.94	++ 0.824	- 0.39	- 0.412	+++ 0.948

C) Elimination			D) Toxicity						
PMF	$T_{1/2}$ (h)	CL (ml/min/kg)	AMES toxicity	Carcinogenicity	Eye corrosion	Eye irritation	hERG	H-HT	Respiratory toxicity
1	0.529	3.275	+ 0.684	-- 0.145	--- 0.007	++ 0.879	--- 0.022	-- 0.132	-- 0.247

2	0.379	4.228	+ 0.644	-- 0.235	--- 0.012	+++ 0.945	--- 0.053	--- 0.095	+ 0.573
3	0.38	4.36	+ 0.671	--- 0.067	--- 0.004	+ 0.688	--- 0.038	-- 0.208	-- 0.246
4	0.252	4.896	+ 0.638	-- 0.139	--- 0.006	+++ 0.91	--- 0.097	-- 0.122	+ 0.623
5	0.662	6.298	- 0.47	--- 0.034	--- 0.004	-- 0.218	--- 0.034	-- 0.161	-- 0.26
6	0.451	4.368	+ 0.634	-- 0.102	--- 0.006	+ 0.649	--- 0.033	-- 0.178	-- 0.189
7	0.317	5.028	++ 0.709	-- 0.249	--- 0.009	+++ 0.915	-- 0.106	-- 0.129	+ 0.59
8	0.59	6.749	- 0.333	--- 0.032	--- 0.003	--- 0.072	--- 0.045	-- 0.121	-- 0.108
9	0.227	5.899	+ 0.693	-- 0.108	--- 0.005	++ 0.799	-- 0.227	-- 0.15	+ 0.547

CY: Cytochrome; CL: Clearance hERG: Human ether-a-go-go-related gene; H-HT: Human hepatotoxicity

3.7 Correlation analysis of PMFs docked with target proteins

We analyzed the Pearson's correlation between the binding affinity of PMF derivatives to key protein targets and their experimentally determined IC_{50} values against MCF-7 and MDA-MB-231 breast cancer cell lines after 72-hour treatment. A heatmap of Pearson's correlation coefficients (**Figure 15**) revealed a strong positive correlation between the IC_{50} values of PMFs on MCF-7 cells and the binding strength to anti-apoptotic proteins Bcl-XL ($r = 0.831$) and Bcl-2 ($r = 0.773$) and protein mTOR ($r = 0.86$). These findings suggest that PMFs with stronger binding affinity to these proteins tend to exhibit stronger cytotoxicity effect, indicating potential involvement of the target proteins influencing the anticancer activity of PMFs. Conversely, weaker correlations were observed between IC_{50} of PMFs on MDA-MB-231 cells and docking affinities to all protein target, suggesting a different cell line-specific activity profiles, possibly due to differences in target expression levels between ER-positive (MCF-7) and triple-negative (MDA-MB-231) subtypes, as mentioned in the previous section (**3.2**). The strong positive correlations highlight the relevance of apoptosis-related targets in the mode of action of PMFs, in addition to its multitargeted approach in cancer cell death mechanism with the activation of mTOR and cascading downstream markers. The strategies support the use of structure-based multitargeted molecular docking and correlation analysis to validate the lead compounds with promising anticancer potential.

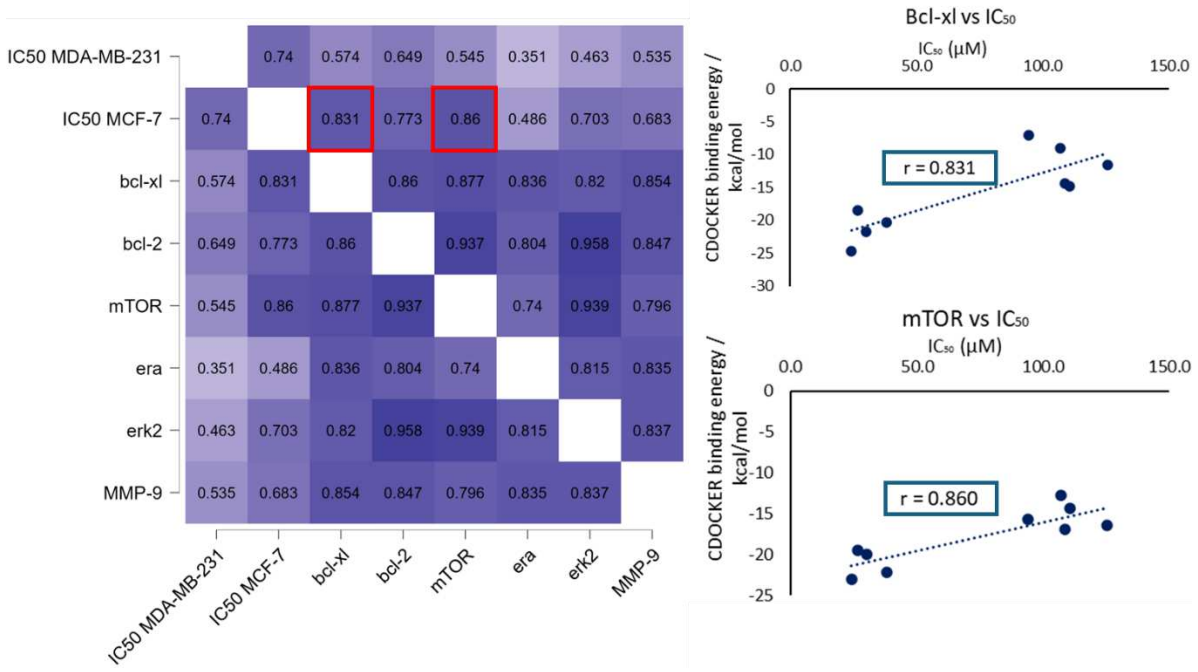

Figure 15 Pearson's correlation analysis heatmap between the experimentally produced IC_{50} of both MCF-7 and MDA-MB-231 breast cancer cell lines and the binding energy of the respective PMFs to the target protein markers.

3.7 Structural-activity relationship (SAR) on anticancer activity of isolated PMFs on MCF-7 breast cancer cell lines

The nine isolated PMFs were split into two major groups, bearing either 5-hydroxy or 5-methoxyflavone derivatives. **PMF 1** to **5** have 5-hydroxy methoxyflavones within its skeleton structure. Meanwhile, **PMF 6** to **9** constitutes 5-methoxyflavones pharmacophore. Among the 5-hydroxy methoxyflavones derivatives, the simplest PMF structure, 5-hydroxy-7-methoxyflavone (**PMF 2**) generates moderate cytotoxic capacity (IC_{50}: 38.20 ± 0.17 μM) after 72-hour treatment (**Figure 5**). The substitution of C4'-OCH_3 yields **PMF 4**, 5-hydroxy-7,4'-dimethoxyflavone with IC_{50} value of 24.12 ± 0.45 μM, the strongest cytotoxicity reported among the isolated PMF. The absence of C4'-OCH_3 group and substitution of C3-OCH_3 yield 5-hydroxy-3,7-dimethoxyflavone (**PMF 1**), with significant reduction in cytotoxic capacity (IC_{50} of 110.62 ± 3.63 μM), when compared to **PMF 2**. Additionally, **PMF 3** (5-hydroxy-3,7,4'-trimethoxyflavone) shows a non-significant improvement in IC_{50} value (IC_{50}: 108.80 ± 1.22 μM) despite the presence of C4'-OCH_3. Based on **Figure 5,** Comparison in IC_{50} of **PMF 3** and **PMF 4** strongly indicates C3-OCH_3 creates an unfavorable effect that led to a significant drop in cytotoxic level. Besides, **PMF 5** (5-hydroxy-3,7,3',4'-tetramethoxyflavone), with disubstituted methoxy group on ring B in C3' and C4' position similarly shows weaker cytotoxic effect with IC_{50} value of 125.52 ± 4.30 μM.

PMF 6 to **9** having 5,7-dimethoxylated within the flavone scaffold (**Figure 16**). Among the four isolated PMFs, **PMF 7** (5,7-dimethoxyflavone) reported moderate IC_{50} value of 30.12 ± 0.85 μM. The presence of C4'-OCH_3 generates a stronger cytotoxicity effect of **PMF 9** (5,7,4'-trimethoxyflavone) with IC_{50} value of 26.69 ± 0.81 μM. Similarly, the existence of C3-OCH_3 significantly weakens the cytotoxic activity of PMFs, with **PMF 6** (3,5,7-trimethoxyflavone) and **PMF 8** (3,5,7,3',4'-pentamethoxyflavone) demonstrated higher IC_{50} value of 106.97 ± 0.63 μM and 94.22 ± 0.70 μM, respectively. The SAR analysis on non-hydroxylated PMF indicates similarities in the promising prospects of C4'-OCH_3 in

improving the cytotoxic capacity of PMF and the unfavored condition of C3-OCH_3 group to the cytotoxic activity as observed on **PMF 6** and **8.**

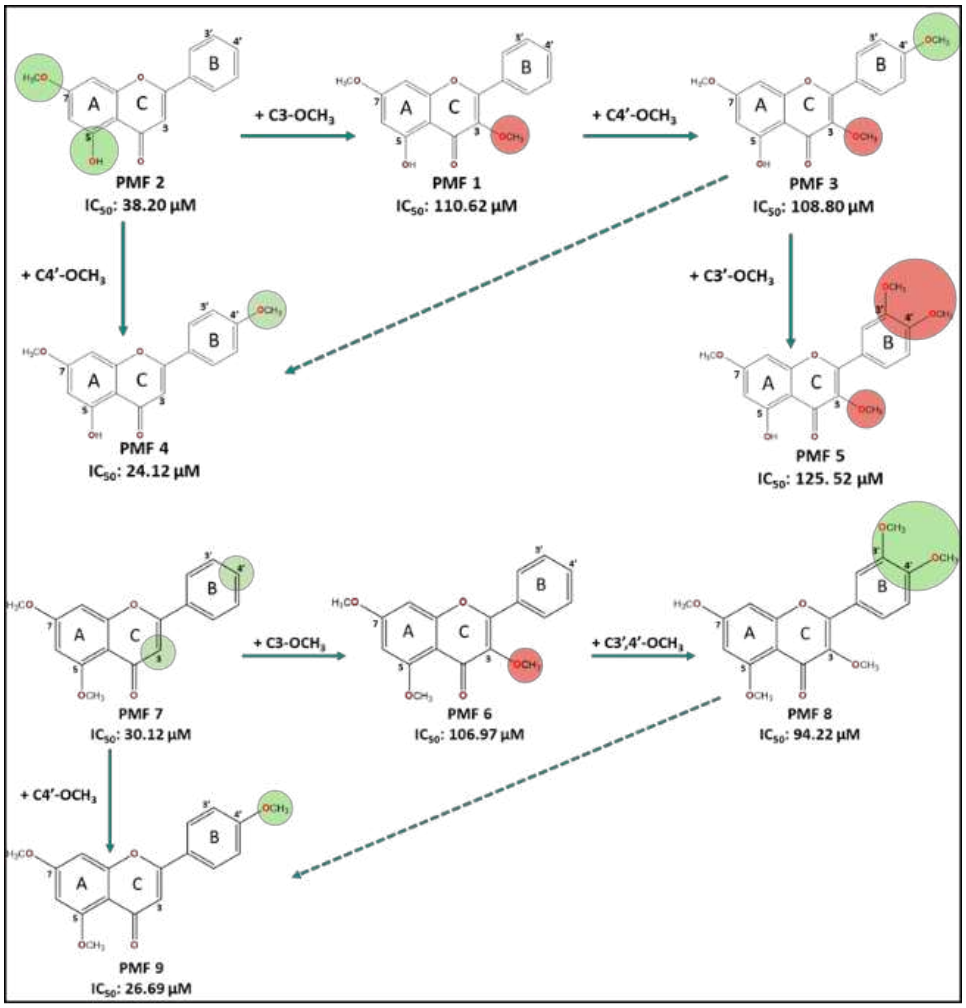

Figure 16 Structural-activity relationship of PMFs derivatives treated against MCF-7 breast cancer cell lines for 72-hour

The hydroxy and methoxy group coexist in the scaffold with distinct chemical properties and synergistically involved in electron donor-acceptor mechanism and influencing electron density distribution within the flavones ring A, B and C (Wang et al., 2024; Zhao et al., 2019). Multiple studies have reported challenges associated with the massive hydrophobic region and extreme lipophilicity of several flavones' derivatives (Xu et al., 2023). Thus, the presence of hydroxy group in some isolated PMF theoretically crucial in expanding the polar region by formation of hydrogen bonds in reducing the lipophilic effect (Hawthorne et al., 2022). Nevertheless, the formation of strong intramolecular hydrogen bonding between the hydroxy group and the carbonyl group hindered HBD potential of C5-OH, and elevated lipophilic capacity (Whaley et al., 2013; Abraham & Mobli, 2007; Whaley et al., 2006). The existence of intramolecular hydrogen bonding was detected and confirmed in ^{1}H-NMR spectrum (Figure) with significant downfield of chemical shift (Horowitz & Trievel, 2012; Scheiner et al., 2000). Additionally, molecular docking and DFT analysis visualized and reaffirmed strong intramolecular hydrogen bonding with bond distance less than 2Å. Interestingly, the lipophilic effect of C5-OH was

greater than the C5-OCH_3 yet demonstrating superior cytotoxic potential (Aidiel et al., 2024). The formation of intramolecular hydrogen bonding acts as a double edge sword in preserving the stability of the compound through resonance effect (**Figure 17**) while partially hindering polar interaction and hydrogen bond donor capability of hydroxyl group (Over et al., 2014; Alex et al., 2011). Nevertheless, the increased hydrophobic and stability by the intramolecular interaction enhanced the membrane permeation in delivery of the compound to the target protein, as observed by the strong cytotoxic activity of PMF 2 and 4 (Hawthorne et al., 2022).

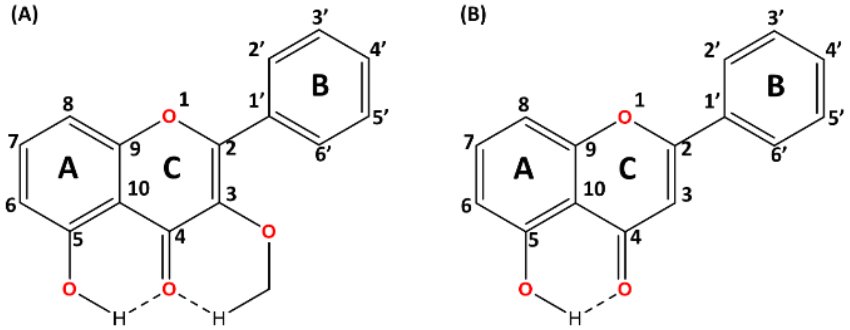

Figure 17 Schematic diagram of potential intramolecular interaction between hydrogen atom of hydroxy group from C3 (**A**) and C5 position (**B**) with the oxygen atom of carbonyl group from C4 position

The strong cytotoxic activity of PMF 2 and PMF 4 with C5-OH ceased with the presence of unfavored C3- and C3'-OCH_3 groups on ring C and B, respectively. The role of C3-OCH_3 in the anticancer activity of PMFs was ambivalent due to limited reports to confirmed. For instance, compounds 5,3'-dihydroxy-3,6,7,8,4'-pentamethoxyflavone demonstrate strong cytotoxic effect on MCF-7 cell lines with IC_{50} value of 3.71 µM in similar treatment duration. However, the results clearly indicate huge contribution of C3'-OH and C4'-OCH_3 in elevating the cytotoxic effect through structural stabilization, hydrogen bond donor capacity and intramolecular interactions of both functional groups (Carcache et al., 2022). Meanwhile, other PMF compounds with C3-OCH_3 group such as calycopterin (5,4'-dihydroxy-3,6,7,8-tetramethoxyflavone), nobiletin and 5-demethylnobiletin demonstrate weak anticancer activity on various cancer cell lines (Tsai et al., 2022; Lotfizadeh et al., 2020). Based on the trends, the weak cytotoxic activity of the isolated PMFs having C3-OCH_3 (**PMF 1**, **3**, **5**, **6** & **8**) would confirm the negative effect of C3-OCH_3 due to several factors.

Firstly, molecular docking analyses indicate PMFs with C3-OCH_3 group initiate weak and transient intramolecular interaction with the carbonyl group at a bond distance exceeds 2.4 Å. Nevertheless, the interaction between both atoms was inconsistent, with **PMF 6** and **8** docked with the estrogen receptor, and **PMF 1** on MMP-9 protein does not yield visible interaction. Based on the electronegativity effect, hydrogen atoms of the methoxy group were not highly polarized when compared to the hydroxy group. Despite poor hydrogen-donating ability of the methoxy group, favourable geometric arrangement and binding site may allow the intrmolecular interaction to occur. The existence of multiple intramolecular interaction with the carbonyl group disrupts the hydrogen bond acceptor capacity and reduces the electrophilic nature carbonyl group, a contributing factor to weakening cytotoxic effect. Secondly, the steric effect of methoxy group could influence and compete with the binding target of carbonyl group, reducing its effectiveness in ligand-receptor interactions. The bulkiness of the methoxy group at C3 might slightly alter the molecular conformation, reducing the accessibility of the C4 carbonyl group for

strong target interactions. If the methoxy group at C3 introduces steric clashes with nearby residues in the binding pocket, it may alter the binding pose and prevent the carbonyl from forming strong protein-ligand interactions. The analysis has been confirmed by multiple studies concerning the effect of hydrophobic group that could influence the binding arrangement of target compound (Bisson et al., 2021). The hypothesis was further supported by stronger cytotoxic effect of **PMF 6** and **8** than its hydroxylated PMFs counterpart, **PMF 1** and **5**. The presence of C5-OH group of **PMF 1** and **5** interferes with hydrogen bond acceptor capacity of the carbonyl group (**Figure 18**). In addition, the possible formation of intramolecular interaction and steric effect arises between C3-OCH_3 and the carbonyl group further hindered the potential main interaction with the amino acid involving carbonyl group, as observed on molecular docking on protein bcl-xl and mTOR.

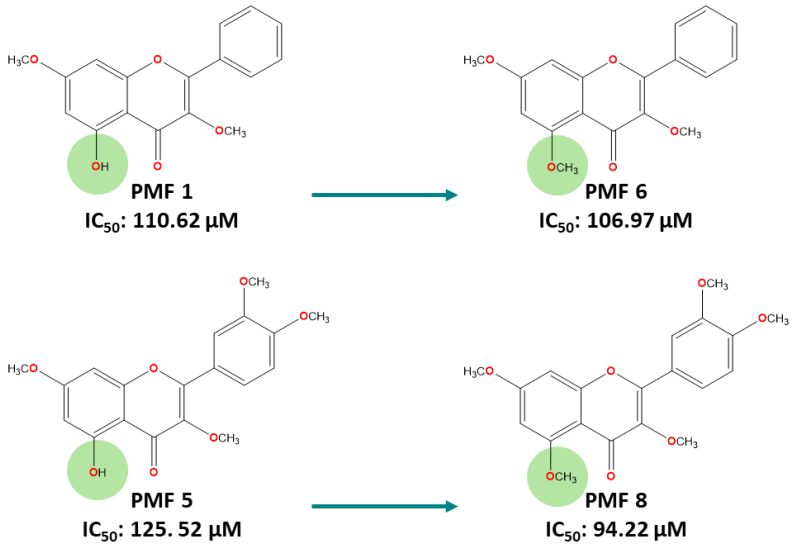

Figure 18 Comparison on IC_{50} value between C5-OH (**PMF 1** & **5**) and C5-OCH_3 (**PMF 6** & **8**) with similar methoxy group substitution.

As the complexity of C5-OH interaction provides a beneficial role in stronger cytotoxic effect on MCF-7 breast cancer cell line, the C5-OCH_3 group on **PMF 6** to **9** delivers distinct advantages. With the absence of intramolecular hydrogen bonding between C5 and C4 atoms position, both functional groups synergistically interact with the target protein in maximizing cytotoxic potential. The C5-OCH_3 roles as the hydrogen bond acceptor and its lipophilic nature initiates a hydrophobic interaction with the proteins (Vongdeth et al., 2019). Nevertheless, the maximum cytotoxic activity of C5-OCH_3 flavones analogs could be achieved with preserved lipophilic capacity on ring B and C. For instance, nobiletin with C5-OCH3 shows weaker anticancer potential compared to tangeritin, due to excessive lipophilic effect on C3 ring C and bulkiness of disubstituted methoxy group on ring B (Chen et al., 2022; Kim et al., 2022; Tsai et al., 2022). With limited roles of C5-OCH_3 group, the hydrogen bond donor capacity of oxygen atom from C4 carbonyl group was a major contributor to strong cytotoxicity effect of these PMFs.

4.0 Conclusion

Breast cancer remains a leading cause of cancer-related death among women globally, especially in Asia. Although current chemotherapeutic drugs like doxorubicin and paclitaxel show strong cytotoxic activity,

they often suffer from poor selectivity and undesirable side effects. Kaempferia parviflora (black ginger), traditionally used in Southeast Asia, contains polymethoxyflavones (PMFs) that have demonstrated potential anticancer properties across various cancer cell lines. This study demonstrates that optimized maceration extraction of *K. parviflora* yields bioactive PMFs with significant anticancer potential. **PMF 4**, **7**, and **9** were the most cytotoxic to breast cancer cell lines, whereas **PMF 9** with the least non-toxic effect on NIH-3T3 normal mouse fibroblast. Based on the structural-activity relationship (SAR), specific methoxy substitutions on PMFs structures significantly influence cytotoxic efficacy. For instance, the presence of C5-OH and C4'-OCH_3 groups enhanced the cytotoxic effects, while bulky substitutions on phenyl ring B and C3-OCH_3 group diminished the efficacy. The *in silico* investigation via molecular docking results validated the multitarget mechanism of PMFs inducing apoptosis via the intrinsic mitochondrial pathway. The DFT investigation further reaffirmed the electronic properties of PMFs as a highly stabilized electron-acceptor compound that assists in stronger interaction with the targeted apoptotic proteins. Drug-likeness and ADMET screening validate the bioavailability and safety profile of the PMF. Therefore, **PMF 4**, **7** and **9** emerged as a promising candidate for further development as therapeutic agent in cancer.

Author Contributions

Conceptualization, M.A. and M.A.M.; methodology, M.A., M.A.M.; validation, M.A., M.A.M.; formal analysis, M.A. and M.A.M.; investigation, M.A., M.A.M.; resources, M.A.M.; data curation, M.A., M.A.M.; writing—original draft preparation, M.A., M.A.M.; writing—review and editing, M.A., M.A.M.; visualization, M.A.; supervision, M.A.M.; project administration, M.A., M.A.M. All authors have read and agreed to the published version of the manuscript.

Funding

This work was supported by the Management & Science University.

Institutional Review Board Statement

Not applicable.

Informed Consent Statement

Not applicable.

Data Availability Statement

The raw data supporting the conclusions of this article will be made available by the authors on request.

Conflicts of Interest

The authors declare no conflicts of interest.

Acknowledgement

The author also thanks to Science Officers from the Management & Science University, Mr. Yusof, Mr. Azizan and Mr. Zarifi and Science Technologist from the Department of Pathology, Faculty of Medicine and Health Science, University Putra Malaysia, Mdm. Ummu Raihan, Mdm. Marsitah and Mdm. Farizatul for the technical support in the completion of this project.

References

Abraham, R. J., & Mobli, M. (2007). An NMR, IR and theoretical investigation of 1H Chemical Shifts and hydrogen bonding in phenols. *Magnetic Resonance in Chemistry*, *45*(10), 865–877. https://doi.org/10.1002/mrc.2060

Acharya, R., Chacko, S., Bose, P., Lapenna, A., & Pattanayak, S. P. (2019). Structure Based Multitargeted Molecular Docking Analysis of Selected Furanocoumarins against Breast Cancer. *Scientific Reports*, *9*(1). https://doi.org/10.1038/s41598-019-52162-0

Afridi, M. B., Sardar, H., Serdaroğlu, G., Shah, S. W. A., Alsharif, K. F., & Khan, H. (2024). SwissADME studies and Density Functional Theory (DFT) approaches of methyl substituted curcumin derivatives. *Computational Biology and Chemistry*, *112*, 108153. https://doi.org/10.1016/j.compbiolchem.2024.108153

Agu, P. C., Afiukwa, C. A., Orji, O. U., Ezeh, E. M., Ofoke, I. H., Ogbu, C. O., Ugwuja, E. I., & Aja, P. M. (2023). Molecular docking as a tool for the discovery of molecular targets of nutraceuticals in diseases management. *Scientific Reports*, *13*(1). https://doi.org/10.1038/s41598-023-40160-2

Ahmad, I., Jagatap, V., & Patel, H. (2023). Application of density functional theory (DFT) and response surface methodology (RSM) in drug discovery. In *Elsevier eBooks* (pp. 371–392). https://doi.org/10.1016/b978-0-323-90593-0.00004-6

Aidiel, M., Abdul Mutalib, M., Azman, A. K., Khalid, K., Nik Ramli, N. N., Ramasamy, R., Tang, S. G. H., & Adam, S. H. (2024). Enhancing the total polyphenol content and antioxidant activity of Kaempferia parviflora through optimized binary solvent extraction: isolation and characterization of major PMF metabolite. *Malaysia Journal of Chemistry*, *26*(6). https://doi.org/10.55373/mjchem.v26i6.106

Aidiel, M., Maisarah, A., Khalid, K., Ramli, N. N., Tang, S., & Adam, S. (2023). Polymethoxyflavones transcends expectation, a prominent flavonoid subclass from Kaempferia parviflora: A critical review. *Arabian Journal of Chemistry*, *17*(1), 105364. https://doi.org/10.1016/j.arabjc.2023.105364

Aidiel, M., Mutalib, M. A., Ramasamy, R., Ramli, N. N. N., Tang, S. G. H., & Adam, S. H. (2025). Mechanistic Insights into the Anticancer Potential of Methoxyflavones Analogs: A Review. *Molecules*, *30*(2), 346. https://doi.org/10.3390/molecules30020346

Akl, M. A., Mostafa, A. G., El-Zeny, A. S., & El-Gharkawy, E. R. H. (2025). Design, spectroscopic analysis, DFT calculations, adsorption evaluation, molecular docking, comprehensive in silico and in vitro bioactivity studies of thiocarbohydrazide grafted dialdehyde cellulose nanobiosorbent. *Scientific Reports*, *15*(1). https://doi.org/10.1038/s41598-025-96525-2

Alex, A., Millan, D. S., Perez, M., Wakenhut, F., & Whitlock, G. A. (2011). Intramolecular hydrogen bonding to improve membrane permeability and absorption in beyond rule of five chemical space. *MedChemComm*, *2*(7), 669. https://doi.org/10.1039/c1md00093d

Atanasov, A. G., Zotchev, S. B., Dirsch, V. M., Orhan, I. E., Banach, M., Rollinger, J. M., Barreca, D., Weckwerth, W., Bauer, R., Bayer, E. A., Majeed, M., Bishayee, A., Bochkov, V., Bonn, G. K., Braidy, N., Bucar, F., Cifuentes, A., D'Onofrio, G., Bodkin, M., . . . Supuran, C. T. (2021). Natural products in drug discovery: advances and opportunities. *Nature Reviews Drug Discovery*, *20*(3), 200–216. https://doi.org/10.1038/s41573-020-00114-z

Bakale, R. D., Sulakhe, S. M., Kasare, S. L., Sathe, B. P., Rathod, S. S., Choudhari, P. B., Rekha, E. M., Sriram, D., & Haval, K. P. (2023). Design, synthesis and antitubercular assessment of 1, 2, 3-triazole incorporated thiazolylcarboxylate derivatives. *Bioorganic & Medicinal Chemistry Letters*, *97*, 129551. https://doi.org/10.1016/j.bmcl.2023.129551

Bakht, M. A., Ali, I., & Singh, G. (2024). Green synthesis, density functional theory (DFT), molecular docking, molecular dynamics simulation and biological activity of 1,2,3,4-tetrahydropyrimidine-5-carbonitrile derivatives as PLA2 and proteinase K inhibitors. *Arabian Journal of Chemistry*, *17*(6), 105798. https://doi.org/10.1016/j.arabjc.2024.105798

Becke, A. D. (1988). Density-functional exchange-energy approximation with correct asymptotic behavior. *Physical Review. A, General Physics*, *38*(6), 3098–3100. https://doi.org/10.1103/physreva.38.3098

Bhatia, M. (2023). An overview of conceptual-DFT based insights into global chemical reactivity of volatile sulfur compounds (VSCs). *Computational Toxicology*, *29*, 100295. https://doi.org/10.1016/j.comtox.2023.100295

Bisson, C., Salmon, R. C., West, L., Rafferty, J. B., Hitchcock, A., Thomas, G. H., & Kelly, D. J. (2021). The structural basis for high-affinity uptake of lignin-derived aromatic compounds by proteobacterial TRAP transporters. *FEBS Journal*, *289*(2), 436–456. https://doi.org/10.1111/febs.16156

Bursch, M., Mewes, J., Hansen, A., & Grimme, S. (2022). Best-Practice DFT Protocols for Basic Molecular Computational Chemistry**. *Angewandte Chemie International Edition*, *61*(42). https://doi.org/10.1002/anie.202205735

Carcache, P. J. B., Eugenio, G. D. A., Ninh, T. N., Moore, C. E., Rivera-Chávez, J., Ren, Y., Soejarto, D. D., & Kinghorn, A. D. (2022). Cytotoxic constituents of Glycosmis ovoidea collected in Vietnam. *Fitoterapia*, *162*, 105265. https://doi.org/10.1016/j.fitote.2022.105265

Chen, D., Li, H., Li, W., Feng, S., & Deng, D. (2018). Kaempferia parviflora and Its Methoxyflavones: Chemistry and Biological Activities. *Evidence-based Complementary and Alternative Medicine*, *2018*(1). https://doi.org/10.1155/2018/4057456

Chen, P., Wang, C., Tsao, E., Chen, Y., Wu, M., Ho, C., & Yen, J. (2022). 5-Demethylnobiletin inhibits cell proliferation, downregulates ID1 expression, modulates the NF-KB/TNF-A pathway and exerts antileukemic effects in AML cells. *International Journal of Molecular Sciences*, *23*(13), 7392. https://doi.org/10.3390/ijms23137392

Daina, A., Michielin, O., & Zoete, V. (2017). SwissADME: a free web tool to evaluate pharmacokinetics, drug-likeness and medicinal chemistry friendliness of small molecules. *Scientific Reports*, *7*(1). https://doi.org/10.1038/srep42717

Deb, P. K., Al-Shar'i, N. A., Venugopala, K. N., Pillay, M., & Borah, P. (2021). In vitro anti-TB properties, in silico target validation, molecular docking and dynamics studies of substituted

1,2,4-oxadiazole analogues against Mycobacterium tuberculosis. *Journal of Enzyme Inhibition and Medicinal Chemistry*, *36*(1), 869–884. https://doi.org/10.1080/14756366.2021.1900162

Ding, Y., & Xue, X. (2024). Medicinal chemistry strategies for the modification of bioactive natural products. *Molecules*, *29*(3), 689. https://doi.org/10.3390/molecules29030689

Elkaeed, E. B., Yousef, R. G., Elkady, H., Gobaara, I. M. M., Alsfouk, B. A., Husein, D. Z., Ibrahim, I. M., Metwaly, A. M., & Eissa, I. H. (2022). Design, Synthesis, Docking, DFT, MD Simulation studies of a new Nicotinamide-Based derivative: in vitro anticancer and VEGFR-2 inhibitory effects. *Molecules*, *27*(14), 4606. https://doi.org/10.3390/molecules27144606

Elkhalifa, A. E. O., Al-Shammari, E., Kuddus, M., Adnan, M., Sachidanandan, M., Awadelkareem, A. M., Qattan, M. Y., Khan, M. I., Abduljabbar, S. I., Baig, M. S., & Ashraf, S. A. (2023). Structure-Based Multi-Targeted molecular docking and dynamic simulation of Soybean-Derived isoflavone genistin as a potential breast cancer signaling proteins inhibitor. *Life*, *13*(8), 1739. https://doi.org/10.3390/life13081739

Ertl, P. (2021). Substituents of life: The most common substituent patterns present in natural products. *Bioorganic & Medicinal Chemistry*, *54*, 116562. https://doi.org/10.1016/j.bmc.2021.116562

Fargher, H. A., Sherbow, T. J., Haley, M. M., Johnson, D. W., & Pluth, M. D. (2022). C–H···S hydrogen bonding interactions. *Chemical Society Reviews*, *51*(4), 1454–1469. https://doi.org/10.1039/d1cs00838b

Franchi, M., Piperigkou, Z., Karamanos, K., Franchi, L., & Masola, V. (2020). Extracellular Matrix-Mediated breast cancer cells morphological alterations, invasiveness, and Microvesicles/Exosomes release. *Cells*, *9*(9), 2031. https://doi.org/10.3390/cells9092031

Gest, C., Joimel, U., Huang, L., Pritchard, L., Petit, A., Dulong, C., Buquet, C., Hu, C., Mirshahi, P., Laurent, M., Fauvel-Lafève, F., Cazin, L., Vannier, J., Lu, H., Soria, J., Li, H., Varin, R., & Soria, C. (2013). Rac3 induces a molecular pathway triggering breast cancer cell aggressiveness: differences in MDA-MB-231 and MCF-7 breast cancer cell lines. *BMC Cancer*, *13*(1). https://doi.org/10.1186/1471-2407-13-63

Gjerdrum, C., Tiron, C., Høiby, T., Stefansson, I., Haugen, H., Sandal, T., Collett, K., Li, S., McCormack, E., Gjertsen, B. T., Micklem, D. R., Akslen, L. A., Glackin, C., & Lorens, J. B.

(2009). Axl is an essential epithelial-to-mesenchymal transition-induced regulator of breast cancer metastasis and patient survival. *Proceedings of the National Academy of Sciences*, *107*(3), 1124–1129. https://doi.org/10.1073/pnas.0909333107

Ha, T. T. T., Dung, N. T., Trung, K. H., Tai, B. H., & Van Kiem, P. (2023). Phytochemical constituents from the rhizomes of *Kaempferia parviflora* Wall. ex Baker and their acetylcholinesterase inhibitory activity. *Natural Product Research*, *38*(6), 994–1001. https://doi.org/10.1080/14786419.2023.2210738

Hadi, N. a. A., Kamarulzaman, S. A., Adam, S. H., & Ramli, N. N. N. (2025). Mitigation of oxidative stress and testicular damage by Barringtonia racemosa aqueous extract in streptozotocin-nicotinamide induced diabetic rats. *Asia-Pacific Journal of Molecular Biology and Biotechnology*, 37–44. https://doi.org/10.35118/apjmbb.2025.033.1.05

Hawthorne, D., Pannala, A., Sandeman, S., & Lloyd, A. (2022). Sustained and targeted delivery of hydrophilic drug compounds: A review of existing and novel technologies from bench to bedside. *Journal of Drug Delivery Science and Technology*, *78*, 103936. https://doi.org/10.1016/j.jddst.2022.103936

Holliday, D. L., & Speirs, V. (2011). Choosing the right cell line for breast cancer research. *Breast Cancer Research*, *13*(4). https://doi.org/10.1186/bcr2889

Horowitz, S., & Trievel, R. C. (2012). Carbon-Oxygen hydrogen bonding in biological structure and function. *Journal of Biological Chemistry*, *287*(50), 41576–41582. https://doi.org/10.1074/jbc.r112.418574

Huo, T., Zhao, X., Cheng, Z., Wei, J., Zhu, M., Dou, X., & Jiao, N. (2023). Late-stage modification of bioactive compounds: Improving druggability through efficient molecular editing. *Acta Pharmaceutica Sinica B*, *14*(3), 1030–1076. https://doi.org/10.1016/j.apsb.2023.11.021

Jamtsho, T., Yeshi, K., Perry, M. J., Loukas, A., & Wangchuk, P. (2024). Approaches, Strategies and Procedures for Identifying Anti-Inflammatory Drug Lead Molecules from Natural Products. *Pharmaceuticals*, *17*(3), 283. https://doi.org/10.3390/ph17030283

Jensen, F. (2012). Atomic orbital basis sets. *Wiley Interdisciplinary Reviews Computational Molecular Science*, *3*(3), 273–295. https://doi.org/10.1002/wcms.1123

Jiang, W. G., & Mansel, R. E. (2000). E-cadherin complex and its abnormalities in human breast cancer. *Surgical Oncology*, *9*(4), 151–171. https://doi.org/10.1016/s0960-7404(01)00010-x

Kim, E., Kim, Y., Ji, Z., Kang, J. M., Wirianto, M., Paudel, K. R., Smith, J. A., Ono, K., Kim, J., Eckel-Mahan, K., Zhou, X., Lee, H. K., Yoo, J. Y., Yoo, S., & Chen, Z. (2022). ROR activation by Nobiletin enhances antitumor efficacy via suppression of IκB/NF-κB signaling in triple-negative breast cancer. *Cell Death and Disease*, *13*(4). https://doi.org/10.1038/s41419-022-04826-5

Lee, C., Yang, W., & Parr, R. G. (1988). Development of the Colle-Salvetti correlation-energy formula into a functional of the electron density. *Physical Review. B, Condensed Matter*, *37*(2), 785–789. https://doi.org/10.1103/physrevb.37.785

Lee, M., Han, A., Jang, M., Choi, H., Lee, S., Kim, K., & Lim, T. (2018). Antiskin Inflammatory Activity of Black Ginger (Kaempferia parviflora) through Antioxidative Activity. *Oxidative Medicine and Cellular Longevity*, *2018*(1). https://doi.org/10.1155/2018/5967150

Lee, S., Jang, T., Kim, K. H., & Kang, K. S. (2022). Improvement of Damage in Human Dermal Fibroblasts by 3,5,7-Trimethoxyflavone from Black Ginger (Kaempferia parviflora). *Antioxidants*, *11*(2), 425. https://doi.org/10.3390/antiox11020425

Lim, D. W., Lee, J., Lee, C., & Kim, Y. T. (2024). Natural products and their neuroprotective effects in degenerative brain diseases: A comprehensive review. *International Journal of Molecular Sciences*, *25*(20), 11223. https://doi.org/10.3390/ijms252011223

Łodyga-Chruścińska, E., Kowalska-Baron, A., Błazińska, P., Pilo, M., Zucca, A., Korolevich, V. M., & Cheshchevik, V. T. (2019). Position impact of hydroxy groups on spectral, Acid–Base profiles and DNA interactions of several monohydroxy flavanones. *Molecules*, *24*(17), 3049. https://doi.org/10.3390/molecules24173049

Lohitha, N., Kumar, P. H., Sarveswari, S., Rathod, S., Chaudhari, S., Tamboli, Y., Islam, I., & Vijayakumar, V. (2024). Synthesis, characterization, in silico DFT, molecular docking, and dynamics simulation studies of phenylhydrazono phenoxyquinolones for their hypoglycemic efficacy. *ACS Omega*, *9*(14), 16384–16399. https://doi.org/10.1021/acsomega.4c00079

LoPachin, R. M., & Gavin, T. (2015). Reactions of electrophiles with nucleophilic thiolate sites: relevance to pathophysiological mechanisms and remediation. *Free Radical Research*, *50*(2), 195–205. https://doi.org/10.3109/10715762.2015.1094184

LoPachin, R. M., Geohagen, B. C., & Nordstroem, L. U. (2019). Mechanisms of soft and hard electrophile toxicities. *Toxicology*, *418*, 62–69. https://doi.org/10.1016/j.tox.2019.02.005

Lotfizadeh, R., Sepehri, H., Attari, F., & Delphi, L. (2020). Flavonoid calycopterin induces apoptosis in human prostate cancer cells in-vitro. *Iranian Journal of Pharmaceutical Research*, *19*(3), 391–401. https://doi.org/10.22037/ijpr.2020.113410.14283

Luan, N., Tuan, N., Dam, N., Hoa, T., Tinh, T., & Minh, N. (2020). Extraction, isolation and identification of four methoxyflavones from leaves of Muntingia calabura L. *Can Tho University Journal of Science*, *Vol.11(1)*, 58. https://doi.org/10.22144/ctu.jen.2020.008

Mahmoodi, N., Bayat, M., Gheidari, D., & Sadeghian, Z. (2024). In silico evaluation of cis-dihydroxy-indeno[1,2-d]imidazolones as inhibitors of glycogen synthase kinase-3: synthesis, molecular docking, physicochemical data, ADMET,MD simulation, and DFT calculations. *Journal of Saudi Chemical Society*, *28*(4), 101894. https://doi.org/10.1016/j.jscs.2024.101894

Martin, T. A., Ye, L., Sanders, A. J., Lane, J., & Jiang, W. G. (2013). *Cancer Invasion and Metastasis: Molecular and Cellular perspective*. Madame Curie Bioscience Database - NCBI Bookshelf. https://www.ncbi.nlm.nih.gov/books/NBK164700/

McREE, D. E. (1999). COMPUTATIONAL TECHNIQUES. In *Elsevier eBooks* (pp. 91-cp1). https://doi.org/10.1016/b978-012486052-0/50005-1

Mushtaq, Z., Aslam, M., Imran, M., Abdelgawad, M. A., Saeed, F., Khursheed, T., Umar, M., Abdulmonem, W. A., Ghorab, A. H. A., Alsagaby, S. A., Tufail, T., Raza, M. A., Hussain, M., & JBawi, E. A. (2023). Polymethoxyflavones: an updated review on pharmacological properties and underlying molecular mechanisms. *International Journal of Food Properties*, *26*(1), 866–893. https://doi.org/10.1080/10942912.2023.2189568

Mutalib, M. A., Shamsuddin, A. S., Ramli, N. N. N., Tang, S. G. H., & Adam, S. H. (2023). Antiproliferative activity and polyphenol analysis in tomato (Solanum lycopersicon).

Malaysian Journal of Microscopy, *19*(1). https://malaysianjournalofmicroscopy.org/ojs/index.php/mjm/article/view/737

Nanda, V., & Schmiedekamp, A. (2007). Are aromatic carbon donor hydrogen bonds linear in proteins? *Proteins Structure Function and Bioinformatics*, *70*(2), 489–497. https://doi.org/10.1002/prot.21537

Neese, F. (2011). The ORCA program system. *Wiley Interdisciplinary Reviews Computational Molecular Science*, *2*(1), 73–78. https://doi.org/10.1002/wcms.81

Neese, F. (2022). Software update: The ORCA program system—Version 5.0. *Wiley Interdisciplinary Reviews Computational Molecular Science*, *12*(5). https://doi.org/10.1002/wcms.1606

Neese, F., Wennmohs, F., Becker, U., & Riplinger, C. (2020). The ORCA quantum chemistry program package. *The Journal of Chemical Physics*, *152*(22). https://doi.org/10.1063/5.0004608

Nohara, K., Wang, F., & Spiegel, S. (1998). Glycosphingolipid composition of MDA-MB-231 and MCF-7 human breast cancer cell lines. *Breast Cancer Research and Treatment*, *48*(2), 149–157. https://doi.org/10.1023/a:1005986606010

Oselusi, S. O., Dube, P., Odugbemi, A. I., Akinyede, K. A., Ilori, T. L., Egieyeh, E., Sibuyi, N. R., Meyer, M., Madiehe, A. M., Wyckoff, G. J., & Egieyeh, S. A. (2024). The role and potential of computer-aided drug discovery strategies in the discovery of novel antimicrobials. *Computers in Biology and Medicine*, *169*, 107927. https://doi.org/10.1016/j.compbiomed.2024.107927

Over, B., McCarren, P., Artursson, P., Foley, M., Giordanetto, F., Grönberg, G., Hilgendorf, C., Lee, M. D., Matsson, P., Muncipinto, G., Pellisson, M., Perry, M. W. D., Svensson, R., Duvall, J. R., & Kihlberg, J. (2014). Impact of stereospecific intramolecular hydrogen bonding on cell permeability and physicochemical properties. *Journal of Medicinal Chemistry*, *57*(6), 2746–2754. https://doi.org/10.1021/jm500059t

Paramee, S., Sookkhee, S., Sakonwasun, C., Takuathung, M. N., Mungkornasawakul, P., Nimlamool, W., & Potikanond, S. (2018). Anti-cancer effects of Kaempferia parviflora on ovarian cancer SKOV3 cells. *BMC Complementary and Alternative Medicine*, *18*(1). https://doi.org/10.1186/s12906-018-2241-6

Parekh, A., Das, D., Das, S., Dhara, S., Biswas, K., Mandal, M., & Das, S. (2018). Bioimpedimetric analysis in conjunction with growth dynamics to differentiate aggressiveness of cancer cells. *Scientific Reports*, *8*(1). https://doi.org/10.1038/s41598-017-18965-9

Peng, Q., Zhang, Y., Zhu, M., Bao, F., Deng, J., & Li, W. (2022). Polymethoxyflavones from citrus peel: advances in extraction methods, biological properties, and potential applications. *Critical Reviews in Food Science and Nutrition*, *64*(16), 5618–5630. https://doi.org/10.1080/10408398.2022.2156476

Phung, H. M., Lee, S., Hong, S., Lee, S., Jung, K., & Kang, K. S. (2021). Protective Effect of Polymethoxyflavones Isolated from Kaempferia parviflora against TNF-α-Induced Human Dermal Fibroblast Damage. *Antioxidants*, *10*(10), 1609. https://doi.org/10.3390/antiox10101609

Sae-Wong, C., Matsuda, H., Tewtrakul, S., Tansakul, P., Nakamura, S., Nomura, Y., & Yoshikawa, M. (2011). Suppressive effects of methoxyflavonoids isolated from Kaempferia parviflora on inducible nitric oxide synthase (iNOS) expression in RAW 264.7 cells. *Journal of Ethnopharmacology*, *136*(3), 488–495. https://doi.org/10.1016/j.jep.2011.01.013

Sae-Wong, C., Tansakul, P., & Tewtrakul, S. (2009). Anti-inflammatory mechanism of Kaempferia parviflora in murine macrophage cells (RAW 264.7) and in experimental animals. *Journal of Ethnopharmacology*, *124*(3), 576–580. https://doi.org/10.1016/j.jep.2009.04.059

Scheiner, S., Gu, Y., & Kar, T. (2000). Evaluation of the H-bonding properties of CH···O interactions based upon NMR spectra. *Journal of Molecular Structure THEOCHEM*, *500*(1–3), 441–452. https://doi.org/10.1016/s0166-1280(00)00375-4

Seo, S., Lee, Y., & Moon, H. (2017). Acetyl-cholinesterase Inhibitory Activity of Methoxyflavones Isolated from Kaempferia parviflora. *Natural Product Communications*, *12*(1). https://doi.org/10.1177/1934578x1701200107

Shah, A., Choudhary, A., Jain, M., Perumal, S., Patel, V., Parmar, G., & Patel, A. (2024). Discovery of novel anticancer flavonoids as potential HDAC2 inhibitors: virtual screening approach based on molecular docking, DFT and molecular dynamics simulations studies. *3 Biotech*, *14*(3). https://doi.org/10.1007/s13205-023-03912-5

Shakerzadeh, E. (2016). Theoretical investigations of interactions between boron nitride nanotubes and drugs. In *Elsevier eBooks* (pp. 59–77). https://doi.org/10.1016/b978-0-323-38945-7.00004-3

Shariff, N. F. S. M., Singgampalam, T., Ng, C. H., & Kue, C. S. (2020). Antioxidant activity and zebrafish teratogenicity of hydroalcoholic *Moringa oleifera L*. leaf extracts. *British Food Journal*, 122(10), 3129–3137. https://doi.org/10.1108/bfj-02-2020-0113

Sitthichai, P., Chanpirom, S., Maneerat, T., Charoensup, R., Tree-Udom, T., Pintathong, P., Laphookhieo, S., & Sripisut, T. (2022). Kaempferia parviflora Rhizome Extract as Potential Anti-Acne Ingredient. *Molecules*, *27*(14), 4401. https://doi.org/10.3390/molecules27144401

Snyder, H. D., & Kucukkal, T. G. (2021). Computational Chemistry Activities with Avogadro and ORCA. *Journal of Chemical Education*, *98*(4), 1335–1341. https://doi.org/10.1021/acs.jchemed.0c00959

Sookkhee, S., Sakonwasun, C., Mungkornasawakul, P., Khamnoi, P., Wikan, N., & Nimlamool, W. (2022). Synergistic Effects of Some Methoxyflavones Extracted from Rhizome of Kaempferia parviflora Combined with Gentamicin against Carbapenem-Resistant Strains of Klebsiella pneumoniae, Pseudomonas aeruginosa, and Acinetobacter baumannii. *Plants*, *11*(22), 3128. https://doi.org/10.3390/plants11223128

Sovijit, W., Sovijit, W., Ishii, Y., Kambe, J., Fujita, T., Watanabe, G., Yamaguchi, H., & Nagaoka, K. (2020). Estrogen promotes increased breast cancer cell proliferation and migration through downregulation of CPEB1 expression. *Biochemical and Biophysical Research Communications*, *534*, 871–876. https://doi.org/10.1016/j.bbrc.2020.10.085

Suradej, B., Sookkhee, S., Panyakaew, J., Mungkornasawakul, P., Wikan, N., Smith, D. R., Potikanond, S., & Nimlamool, W. (2019). Kaempferia parviflora Extract Inhibits STAT3 Activation and Interleukin-6 Production in HeLa Cervical Cancer Cells. *International Journal of Molecular Sciences*, *20*(17), 4226. https://doi.org/10.3390/ijms20174226

Thaklaewphan, P., Ruttanapattanakul, J., Monkaew, S., Buatoom, M., Sookkhee, S., Nimlamool, W., & Potikanond, S. (2021). Kaempferia parviflora extract inhibits TNF-α-induced release of

MCP-1 in ovarian cancer cells through the suppression of NF-κB signaling. *Biomedicine & Pharmacotherapy*, *141*, 111911. https://doi.org/10.1016/j.biopha.2021.111911

Theodossiou, T. A., Ali, M., Grigalavicius, M., Grallert, B., Dillard, P., Schink, K. O., Olsen, C. E., Wälchli, S., Inderberg, E. M., Kubin, A., Peng, Q., & Berg, K. (2019). Simultaneous defeat of MCF7 and MDA-MB-231 resistances by a hypericin PDT–tamoxifen hybrid therapy. *Npj Breast Cancer*, *5*(1). https://doi.org/10.1038/s41523-019-0108-8

Tsai, H., Yang, J., Chen, Y., Guo, J., Li, S., Wei, G., Ho, C., Hsu, J., Chang, C., Liang, Y., Yu, H., & Chen, Y. (2022). Acetylation enhances the anticancer activity and oral bioavailability of 5-Demethyltangeretin. *International Journal of Molecular Sciences*, *23*(21), 13284. https://doi.org/10.3390/ijms232113284

Von Szentpály, L., Kaya, S., & Karakuş, N. (2020). Why and When Is Electrophilicity Minimized? New Theorems and Guiding Rules. *The Journal of Physical Chemistry A*, *124*(51), 10897–10908. https://doi.org/10.1021/acs.jpca.0c08196

Vongdeth, K., Han, P., Li, W., & Wang, Q. (2019). Synthesis and antiproliferative activity of natural and Non-Natural polymethoxychalcones and polymethoxyflavones. *Chemistry of Natural Compounds*, *55*(1), 11–17. https://doi.org/10.1007/s10600-019-02605-x

Wang, D., Li, Z., Jiang, Z., Li, Y., Chen, Q., & Zhou, Z. (2024). Polymethoxylated flavone variations and in vitro biological activities of locally cultivated Citrus varieties in China. *Food Chemistry*, *463*, 141047. https://doi.org/10.1016/j.foodchem.2024.141047

Whaley, W. L., Okoso-Amaa, E. M., Womack, C. L., Vladimirova, A., Rogers, L. B., Risher, M. J., & Abraham, M. H. (2013). Summation Solute hydrogen bonding acidity values for hydroxyl substituted flavones determined by NMR spectroscopy. *Natural Product Communications*, *8*(1). https://doi.org/10.1177/1934578x1300800121

Whaley, W. L., Rummel, J. D., & Kastrapeli, N. (2006). Interactions of Genistein and Related Isoflavones with Lipid Micelles. *Langmuir*, *22*(17), 7175–7184. https://doi.org/10.1021/la0606502

Xu, K., Ren, X., Wang, J., Zhang, Q., Fu, X., & Zhang, P. (2023). Clinical development and informatics analysis of natural and semi-synthetic flavonoid drugs: A critical review. *Journal of Advanced Research*, *63*, 269–284. https://doi.org/10.1016/j.jare.2023.11.007

Yagi, M., Hayashi, S., Ishizaki, K., Takabe, W., Inoue, K., Sato, Y., Sakiyama, C., & Yonei, Y. (2019). Inhibitory effect of Kaempferia parviflora Wall. Ex. Baker (Zingiberaceae) rhizome on postprandial hyperglycemia. *Glycative Stress Research*, *6*(2), 126–134. https://doi.org/10.24659/gsr.6.2_126

Zhao, L., Yuan, X., Wang, J., Feng, Y., Ji, F., Li, Z., & Bian, J. (2019). A review on flavones targeting serine/threonine protein kinases for potential anticancer drugs. *Bioorganic & Medicinal Chemistry*, *27*(5), 677–685. https://doi.org/10.1016/j.bmc.2019.01.027

Zhu, W., Wang, Y., Niu, Y., Zhang, L., & Liu, Z. (2023). Current Trends and Challenges in Drug-Likeness Prediction: Are they Generalizable and interpretable? *Health Data Science*, *3*. https://doi.org/10.34133/hds.0098

Zhuang, W., Wang, Y., Cui, P., Xing, L., Lee, J., Kim, D., Jiang, H., & Oh, Y. (2018). Applications of π-π stacking interactions in the design of drug-delivery systems. *Journal of Controlled Release*, *294*, 311–326. https://doi.org/10.1016/j.jconrel.2018.12.014

Zschiesche, W., Schönborn, I., Behrens, J., Herrenknecht, K., Hartveit, F., Lilleng, P., & Birchmeier, W. (1997). Expression of E-cadherin and catenins in invasive mammary carcinomas. *PubMed*, *17*(1B), 561–567. https://pubmed.ncbi.nlm.nih.gov/9066580